Volume 8
Number 15
21 April 2020
Pages 6911–7434

Journal of Materials Chemistry A

Materials for energy and sustainability

rsc.li/materials-a

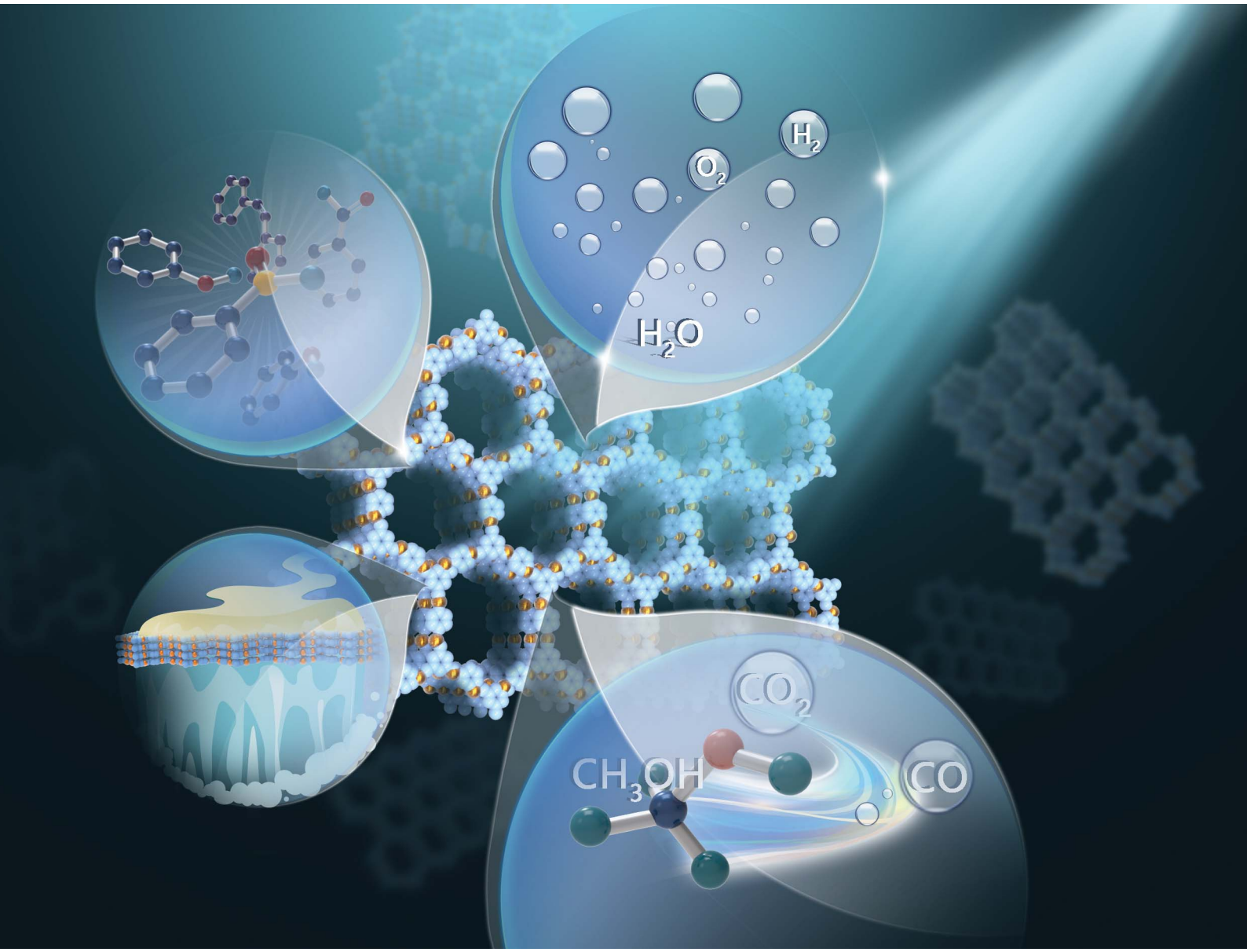

ISSN 2050-7488

ROYAL SOCIETY OF CHEMISTRY

REVIEW ARTICLE

Yan Geng, Yu-Bin Dong *et al.*

Covalent organic frameworks: emerging high-performance platforms for efficient photocatalytic applications

Journal of Materials Chemistry A

ROYAL SOCIETY OF CHEMISTRY

REVIEW

View Article Online
View Journal | View Issue

Cite this: *J. Mater. Chem. A*, 2020, **8**, 6957

Covalent organic frameworks: emerging high-performance platforms for efficient photocatalytic applications

Guang-Bo Wang, Sha Li, Cai-Xin Yan, Fu-Cheng Zhu, Qian-Qian Lin, Ke-Hui Xie, Yan Geng* and Yu-Bin Dong *

Received 14th January 2020
Accepted 5th March 2020

DOI: 10.1039/d0ta00556h

rsc.li/materials-a

Covalent organic frameworks (COFs), as a new emerging class of highly crystalline advanced porous materials with fascinating structural tunability and diversity as well as the desired semiconductor properties, have gained significant attention as highly promising and efficient photocatalysts or designer platforms for a variety of photocatalytic applications in recent years; thus a comprehensive review is timely to summarize the advances of this field. In this review, a background and brief timeline concerning the developments and key achievements of COFs are provided. Afterwards, a systematic overview of the potential photocatalytic applications realized to date in the fast growing field of COFs is provided with the aim of presenting a full blueprint of COFs for possible photochemical energy conversion and reactions. Finally, the challenges remaining and personal perspectives on further development of this type of material for photocatalysis are presented.

1. Introduction

With the booming worldwide growth of the economy, the limited resources and explosive consumption of fossil fuels have caused increasingly serious problems including energy deficiency, global warming and environmental pollution. Tremendous efforts have been devoted to exploring more sustainable alternatives or techniques to address these issues in the past few decades. Among all the potential solutions, visible-light driven photocatalysis, which requires only the inexhaustible and sustainable sunlight as a driving force and an appropriate photocatalyst to conduct the catalytic reactions, is deemed as one of the most promising technologies, and developing more efficient photocatalysts with superior photocatalytic properties is the essence and is of fundamental importance.[1–4] Although the history of photocatalysis dates back to the 1960s,[5,6] the pioneering work by Fujishima and Honda in 1972, in which water splitting was achieved on a TiO_2 electrode under UV light irradiation, was widely recognized as the landmark in the field of photocatalysis.[7] Subsequently, Carey *et al.* reported the photocatalytic decomposition of organic

College of Chemistry, Chemical Engineering and Materials Science, Collaborative Innovation Center of Functionalized Probes for Chemical Imaging in Universities of Shandong, Key Laboratory of Molecular and Nano Probes, Ministry of Education, Shandong Normal University, Jinan 250014, P. R. China. E-mail: gengyan@sdnu.edu.cn; yubindong@sdnu.edu.cn

Dr. Guang-Bo Wang received his Master's degree from Dalian University of Technology in 2014 and obtained his PhD degree in chemistry from Ghent University in 2018. He then moved back to China and joined Shandong Normal University the same year. His current research interests mainly focus on the task-specific design and preparation of advanced crystalline porous materials for photocatalytic applications.

Sha Li was born in Inner Mongolia, China in 1995. She received her BS degree from Inner Mongol Normal University in 2018 and she is currently a Master's candidate in the Dong group at Shandong Normal University. Her research focuses on the construction of novel covalent organic frameworks for photocatalytic hydrogen evolution.

pollutants in the presence of TiO_2 as the photocatalyst[8] and K. Honda for the first time studied the photocatalytic reduction of CO_2 in aqueous suspensions of some semiconductors, including TiO_2, CdS, GaP, ZnO and SiC.[9] Since then, great and fruitful efforts have been made in the rational design and synthesis of different types of inorganic and organic photocatalysts for various photocatalytic applications.[10] The past few decades have witnessed significant progress and burgeoning development in the research field of photocatalysis; however, the amorphous features or lack of long-range order of most photocatalysts limits their photocatalytic efficiency and it is still challenging to determine or formulate the structure–property relationships for materials where their architectures are poorly defined.[11] In this context, the advent of covalent organic frameworks, well known as COFs, has greatly aroused the interest of researchers in multidisciplinary areas of materials science and chemistry in the past few years.

Covalent organic frameworks are a new class of porous, crystalline and extended two- or three-dimensional (2D or 3D) ordered structures that are constructed from molecular organic building blocks entirely composed of light elements (*e.g.* B, C, N and O) and connected by covalent bonds, which are robust and diverse in nature. Since the group of Yaghi reported the first COF material (COF-1) in 2005,[12] this type of well-defined crystalline porous structure has been extensively exploited in a wide range of applications including gas adsorption and separation,[13] heterogeneous catalysis,[14] photodynamic or photothermal therapy,[15,16] sensing[17] and photocatalytic applications.[18] Especially, the discovery of semiconducting COFs by Jiang and co-workers is one of the greatest breakthroughs in both fields of COFs and semiconductors,[19] as it uncovers the great promise of COFs for diverse heterogeneous photocatalysis. In particular, the ordered π columns and high crystallinity of the frameworks can produce pre-organized pathways to facilitate the charge-carrier transport and prevent the charge recombination of the photoexcited states, which indicates the great potential of COFs for optoelectronics and photocatalytic applications. Another distinct feature of COFs is their well-defined molecular backbone, which can be synthetically controlled by altering their linkages, building units and diverse functional groups; this is relatively difficult to achieve with other inorganic and organic semiconductors. With the modularity, porosity, crystallinity, and structural tunability as well as semiconducting properties, in recent years COFs have been realized as efficient platforms for engineering molecular systems to achieve a variety of photocatalytic reactions, such as visible-light driven hydrogen evolution, photocatalytic CO_2 reduction into hydrocarbon fuels, and selective organic reactions as well as the photocatalytic degradation of organic contaminants. So far, most reviews have focused on the design, synthesis and broad applications of COFs with a brief introduction of the photocatalysis based on COF materials;[14,20,21] there is an urgent need to provide a specific review on COFs in the field of photocatalysis from a broad perspective to give a concise, comprehensive and up-to-date overview of the recent developments of this research field. This review starts from the introduction of the chronological development and key achievements in the field of COFs followed by the fundamental principles of photoactive COF-based materials. Then, a detailed and comprehensive overview and discussion of COFs for photocatalytic applications is provided. Finally, some concluding remarks and perspectives on the exploration of COF-based photocatalysts are presented, expecting to stimulate the fast development of more photoactive and promising COFs for diverse photocatalysis applications.

2. Historical developments of COFs

2.1. An overview and chronology of COFs

In 1916, G. N. Lewis for the first time introduced the concept of what would become known as the covalent bond.[22] He outlined a conceptual approach to address the fundamental questions of how atoms can be joined to make molecules; however, it is not

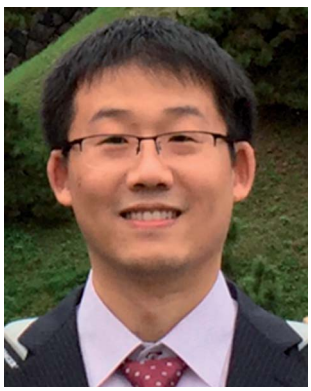

Yan Geng received his B.S. and M.S. in chemistry in 2002 and 2005 from Shandong Normal University under the guidance of Prof. Yu-Bin Dong. He received his Ph.D. in chemistry in 2008 from the Technical Institute of Physics and Chemistry, CAS under the supervision of Prof. Li-Zhu Wu and Prof. Chen-Ho Tung. He then worked at Uppsala University, the University of Queensland, University of Bern and Kyushu University before joining Shandong Normal University in 2017. He is currently a professor focusing on organic materials at the College of Chemistry, Chemical Engineering and Materials Science.

Prof. Yu-Bin Dong is the Chang Jiang professor of chemistry at Shandong Normal University (SDNU). He obtained his PhD from Nankai University (under Prof. Li-Cheng Song) in 1996. He then joined Prof. Andreas Mayr's group at The University of Hong Kong and Prof. Hans-Conrad zur Loye's group at the University of South Carolina from 1996 to 2000, and was promoted to full professor at SDNU in 2000. He is the author of over 200 peer-reviewed publications. His current research interests are in the fields of supramolecular and organometallic chemistry, mainly focusing on MOF and COF-based materials and their applications in catalysis, luminescence, sensing, bioimaging, and cancer treatment.

applicable in controlling how molecules can link together *via* covalent bonds to form extended structures, especially for 2D or 3D covalent organic solids, as highlighted by R. Hoffmann in 1993.[23] The long-standing challenge of extending the dynamic covalent chemistry beyond molecules or one-dimensional (1D) polymers to make covalently linked 2D or 3D crystalline organic structures was finally realized with the first reports of 2D and 3D crystalline COFs in 2005 and 2007 by Yaghi and co-workers, respectively.[12,24] The very first COFs were synthesized by the self-condensation of boronic acids to form boroxine anhydride-based linkages (COF-1) or co-condensation of boronic acids with catechols to form five-membered rings of boronate ester linkages (COF-5); there have been dozens of examples of this type of COF with a diverse set of building units until now.[21] However, boroxine and boronate esters are rather sensitive towards hydrolysis, which immensely limits their further development and possibility for diverse applications. As a result, a variety of different types of reversible reactions and linkages have been exploited and successfully applied to the formation of more stable COFs to date, such as imine-, hydrazone-, azine-, triazine-, amide-, olefin-, dioxin-, sp^2 C=C- and imidazole-linkages (Fig. 1).

Among the various types of COFs, imine-linked COFs *via* Schiff-base reactions of aldehydes and amines are clearly the most widely studied COFs. On the one hand, imine-based COFs exhibit excellent crystallinity, chemical stability and superior structural regularity. On the other hand, imine-linked COFs may chelate with metal ions or complexes due to the nitrogen atoms within the frameworks, which can be potentially employed for heterogeneous catalysis. The first imine-based COF (COF-300) was reported by Yaghi and co-workers in 2009, and was made from tetra-(4-anilyl) methane and terephthalaldehyde (TA) to afford a 3D tetrahedral framework with 5-fold interpenetration.[25] Another subclass of COFs, namely covalent triazine frameworks (CTFs), has been widely studied for diverse applications because of their exceptional chemical stability, nitrogen-rich features and structural tunability along with a high degree of conjugation.[26–29] Typically, CTFs are prepared *via* trimerization of aromatic nitriles under ionothermal conditions[30] or under strong Brønsted acid (CF_3SO_3H) conditions;[31] however, only limited crystalline CTFs have been obtained due to the poor reversibility of the trimerization reactions under the harsh synthesis conditions. Very recently, Tan and co-workers developed a new approach to prepare crystalline CTFs *via* a condensation reaction between aldehydes and amidines, which enhances and broadens both the crystallinity and diversity of CTFs.[32] The structural characterization of COFs was limited to modeling and solutions based on powder X-ray or electron diffraction data until the successful synthesis of single crystal COFs reported by Wang[33] and Dichtel *et al.*[34] in 2018, leading to the unambiguous solution and precise anisotropic refinement. In regard to the photocatalytic applications of COFs, Lotsch and co-workers pioneered the study of COFs for photocatalytic hydrogen evolution under visible-light irradiation by employing a newly designed hydrazone-linked COF as the photocatalyst in the presence of a co-catalyst and sacrificial agent in 2014 (ref. 35) and this work opened up new avenues for COFs to emerge as promising photocatalysts or designer platforms for diverse energy- and environment-related applications. In Fig. 2, we provide a brief chronology of the key achievements made in the field of COFs during the past years and we anticipate that the brief timeline can guide the readers and give them a launching point to this promising and rapidly growing field of COFs and their diverse potential applications.

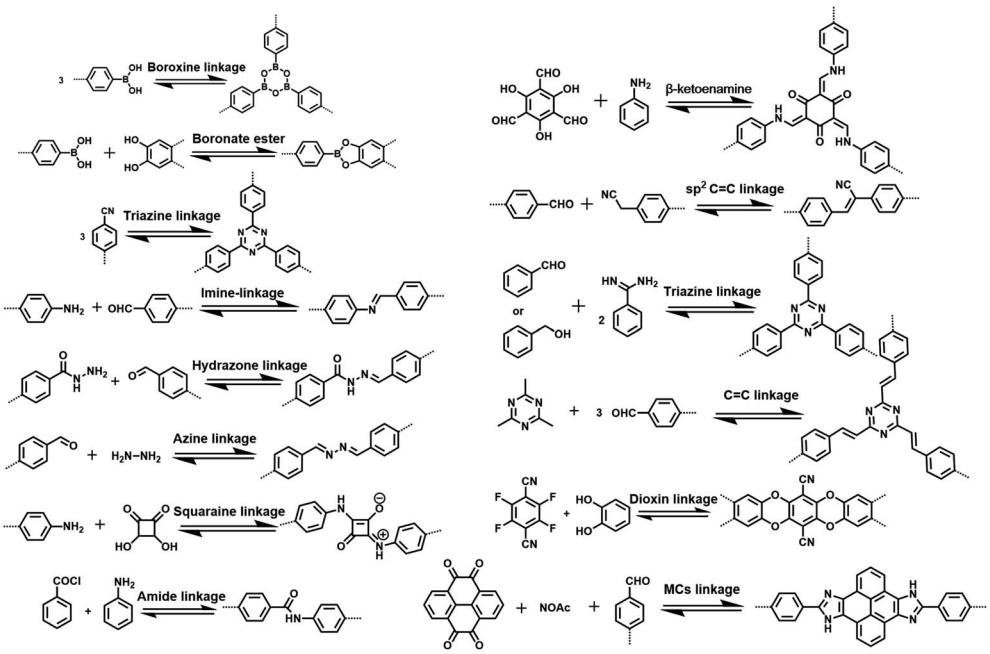

Fig. 1 The most common types of dynamic covalent bonds reported so far for the preparation of COFs.

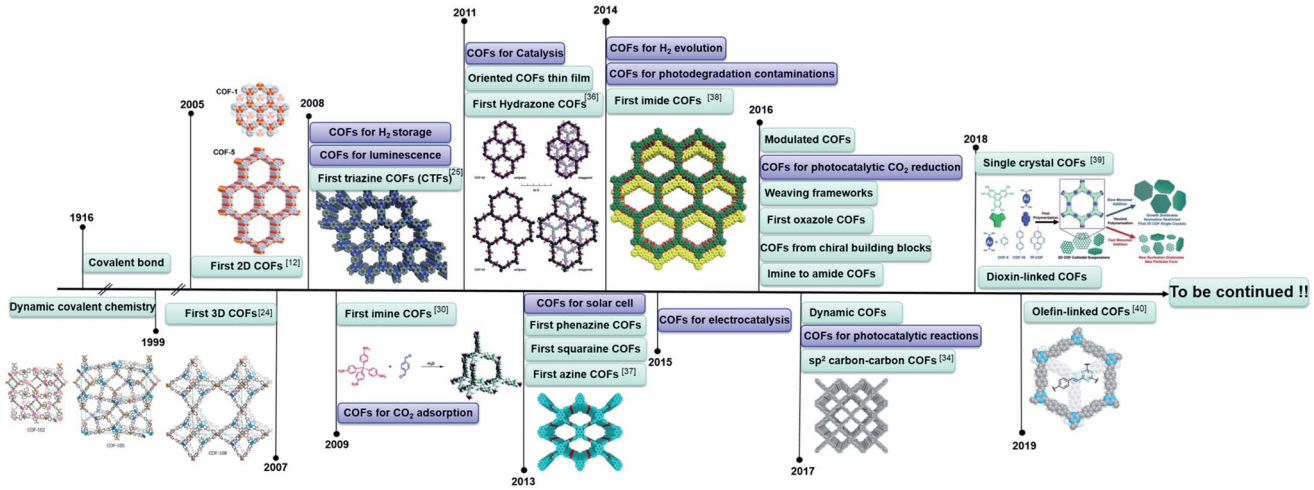

Fig. 2 A brief chronology of the key achievements made in the field of COFs until now. Figures in the chronology were reproduced with permission from ref. 2, 24, 25, 30, 34 and 36–40. Copyright 2005, 2007, 2017, 2018, American Association for the Advancement of Science. Copyright 2008, John Wiley and Sons. Copyright 2009, 2011, 2013, 2019, American Chemical Society. Copyright 2014, Nature Publishing Group.

2.2.1 Fundamental principles of COF-based photocatalysts

Using solar-driven photocatalytic systems to produce valuable energetic fuels for addressing the ever-growing global energy shortage and environmental pollution is attracting massive research attention and developing highly efficient and stable photocatalysts is the essence and of decisive importance for this promising technology. In principle, any photocatalytic reaction involves a series of elementary photochemical processes, including (i) light harvesting, (ii) generation and separation of electron–hole pairs, (iii) migration of photoinduced electrons and holes to the surface, and (iv) surface redox reactions induced by the photogenerated charges, which must be integrated into one molecular system, so that the system can absorb photons to form excitons, the generated excitons can be split into charges, and the charges can be transported to the catalytic centers for the occurrence of the redox reactions. Therefore, light harvesting and band gaps as well as photoexcited charge separation and migration are the key factors affecting the photocatalytic efficiency of a photocatalyst. In this context, an efficient photocatalyst should possess the following features. (1) Excellent photochemical stability. Long-term stability of photocatalysts under light irradiation and the corresponding experimental conditions is the prerequisite for their practical applications. (2) The photocatalyst must have a reasonable band gap and appropriate energy levels of the conduction band (CB) and valence band (VB). Taking photocatalytic water splitting as an example, the bottom level of the CB has to be more negative than the redox potential of H^+/H_2 (0 eV *vs.* normal hydrogen electrode (NHE), pH = 0), while the top level of the VB should be more positive than the redox potential of O_2/H_2O (1.23 eV). Therefore, the theoretical minimum band gap of a photocatalyst for water splitting has to be 1.23 eV, corresponding to a light wavelength of 1100 nm. (3) Superior charge separation and migration of photogenerated carriers. A serious drawback of the existing photocatalysts is their relatively low photocatalytic efficiency because of the fast recombination of the charge carriers. In general, a co-catalyst is commonly added to carry out the proton reduction reaction and a sacrificial electron donor is added to provide the electron source, which can regenerate the photosensitizer by undergoing irreversible decomposition and present back electron transfer. Apart from the aforementioned factors, the porosity, crystallinity, structural diversity and particle sizes of the photocatalysts have also been proven to have great effects on the charge-carrier separation.[1,41] In contrast to other amorphous photocatalysts, the long-range order and π–π conjugated stacks of COFs can not only facilitate rapid mass transport and the exposure of more photoactive sites but can also broaden the light absorption range and promote the transfer of photoexcited excitons, and their optical and electronic properties can be readily tuned due to their structural tunability and diversity; consequently, they exhibit promising photocatalytic activities. In addition, COFs can also serve as ideal platforms to composite with other photoactive species to form heterostructures to further improve the photocatalytic activities of the resulting materials. All these features empower COFs as versatile platforms for task-oriented design and synthesis of efficient photocatalysts.

3. Functional photocatalytic applications

3.1. COFs for photocatalytic hydrogen evolution

Hydrogen, as a sustainable and renewable energy source, is widely deemed as the best alternative to fossil fuels, and achieving hydrogen production through photocatalytic water splitting by using water and sunlight, two sustainable and inexhaustible resources on this planet, is thought to be the essence and of fundamental importance to address the worldwide energy crisis and global warming issues. In recent years, photocatalytic hydrogen evolution using COFs as the

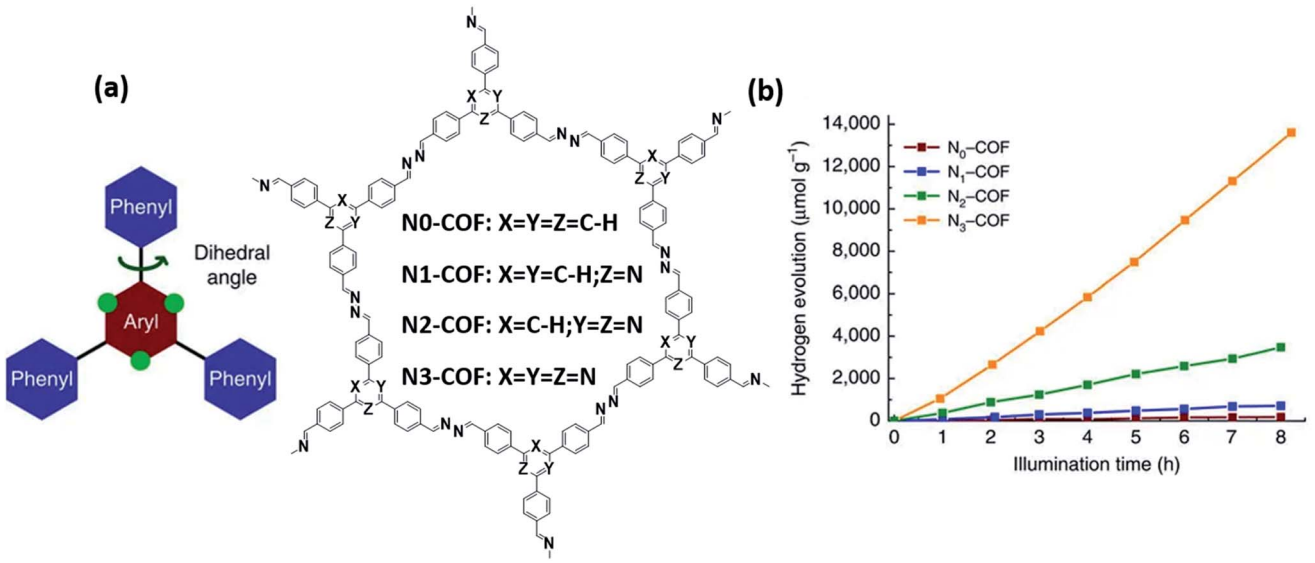

Fig. 3 (a) Schematic representation of the synthesis of N_x-COF. (b) Photocatalytic H_2 evolution during 8 h over the N_x-COF photocatalysts. Adapted from ref. 42 with the permission of Nature Publishing Group, Copyright 2015.

photocatalysts has received increasing research attention and has emerged as a promising hotspot research field.

In an early contribution, Lotsch and co-workers pioneered the application of COFs for photocatalytic hydrogen evolution under visible-light irradiation by the condensation of 2,5-diethoxyterephthalohydrazide (DETH) and 1,3,5-tris(4-formylphenyl) triazine (TFPT) to form a photoactive hydrazone-based COF (TFPT-COF), which can produce H_2 from water with a constant hydrogen evolution rate (HER) of 1970 μmol g^{-1} h^{-1} in the presence of platinum (Pt) nanoparticles and a sacrificial agent of triethanolamine (TEOA).[35] Subsequently, the same group reported a set of azine-linked COFs (N_x-COFs, x = 0–3) with different nitrogen numbers in the central aryl ring (Fig. 3a), which exhibited varied crystallinity and porosity. With Pt as the co-catalyst, a progressively enhanced amount of H_2 was observed with the increase of the nitrogen atoms in the building blocks and the HER was 23, 90, 438 and 1703 μmol g^{-1} h^{-1} for N_0-COF, N_1-COF, N_2-COF and N_3-COF, respectively (Fig. 3b). The enhanced photocatalytic activities were likely derived from the increased surface area and improved charge migration efficiency with more nitrogen atoms in the frameworks.[42] Similarly, they reported three conjugated, photoactive azine-linked COFs based on pyrene building units with different nitrogen atoms in the peripheral aromatic units for photocatalytic hydrogen evolution and their photocatalytic efficiency significantly increased with decreasing number of nitrogen atoms. The photoelectrochemical measurements and quantum-chemical calculations suggested an increase in the thermodynamic driving force with a decrease in the number of nitrogen atoms to be the origin of the observed differences in the HER.[43] These studies strongly confirmed that COFs can be structurally designed and serve as tunable platforms for efficient photocatalytic hydrogen evolution.

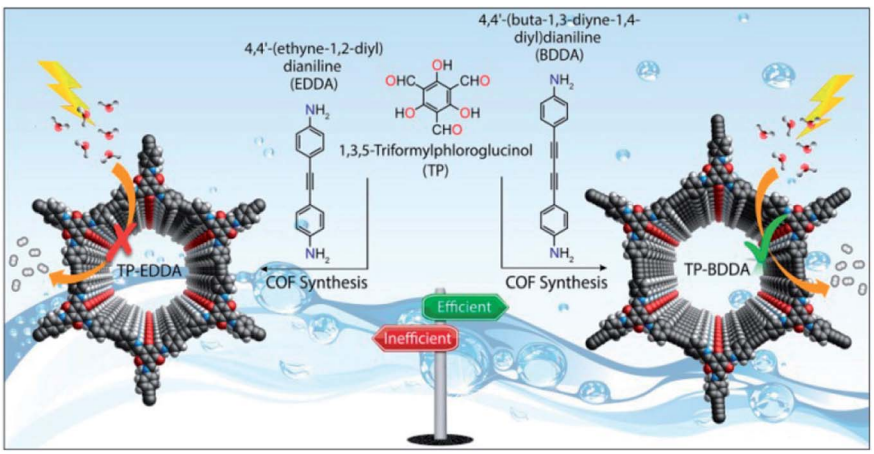

Fig. 4 Schematic illustration of the synthesis of TP-EDDA-COF and TP-BDDA-COF and the photocatalytic hydrogen evolution with them as the photocatalysts under visible-light irradiation. Reproduced from ref. 45 with the permission of the American Chemical Society, Copyright 2018.

To better understand the effects of different functional groups on the overall photocatalytic hydrogen evolution activities of COFs, Sun and co-workers synthesized four β-ketoenamine-based COFs, namely TpPa-COF-X (X = $-(CH_3)_2$, $-CH_3$, –H and $-NO_2$). Under optimized conditions, TpPa-COF-$(CH_3)_2$ exhibited an HER of 8.33 mmol g^{-1} h^{-1} without a significant decrease during 30 h, which is approximately 2.7-fold, 5.3-fold and 38-fold higher than that of TpPa-COF-CH_3 (3.07 mmol g^{-1} h^{-1}), TpPa-COF-H (1.56 mmol g^{-1} h^{-1}) and TpPa-COF-NO_2 (0.22 mmol g^{-1} h^{-1}), respectively. These results revealed that the stronger the electron-donating ability of the functional groups, the better the charge separation efficiency, thus resulting in better photocatalytic performance.[44] Thomas and co-workers constructed two highly crystalline and stable acetylene (–C≡C–) and diacetylene (–C≡C–C≡C–) functionalized β-ketoenamine COFs (TP-EDDA-COF and TP-BDDA-COF, respectively), which were further used as photocatalysts for hydrogen evolution in the presence of Pt as the co-catalyst under visible-light irradiation (Fig. 4). The experimental results showed that the diacetylene moieties had a profound influence on the photocatalytic performance of the COFs as the photocatalytic activity of TP-BDDA-COF (324 μmol g^{-1} h^{-1}) is much higher than that of TP-EDDA-COF (only 30 μmol g^{-1} h^{-1}) under the same conditions.[45]

Very recently, Yu *et al.* reported a thioether-functionalized TTR-COF for photocatalytic hydrogen evolution from seawater for the first time. The specific affinity of thioether to Au ions made the obtained COF material selectively adsorb Au ions, which was thought to be beneficial for separation and migration of the photoexcited electron–hole pairs. As a result, the TTR-COF can selectively capture Au ions over other common transition metal ions and exhibited remarkable photocatalytic activity and stability in seawater. This work highlights the great potential of COFs for practical photocatalytic seawater splitting.[46] In the literature, dibenzo[*b*,*d*]thiophene sulfone has been recognized as one of the most promising building blocks and is widely used for the preparation of conjugated polymers with superior photocatalytic hydrogen evolution activities.[47,48] To study the crucial role of the sulfone units within COF structures, Copper and co-workers synthesized two sulfone functionalized crystalline COFs, termed as S-COF and FS-COF (Fig. 5). For comparison, their related sulfone functionalized conjugated polymers and a sulfone-free counterpart were also prepared. Remarkably, with Pt as the co-catalyst and ascorbic acid as the electron donor, S-COF and FS-COF exhibited an HER of 4.44 and 10.1 mmol g^{-1} h^{-1}, respectively, which was much higher than that of amorphous FS-P (1.12 mmol g^{-1} h^{-1}) and sulfone-free TP-COF (1.60 mmol g^{-1} h^{-1}). The authors ascribed the excellent photocatalytic activity of the COFs to the presence of benzothiophene sulfone moieties. First, the increased planarity of the building blocks can lower the optical band gaps of the COFs, thus increasing their light absorption ability and excited-state

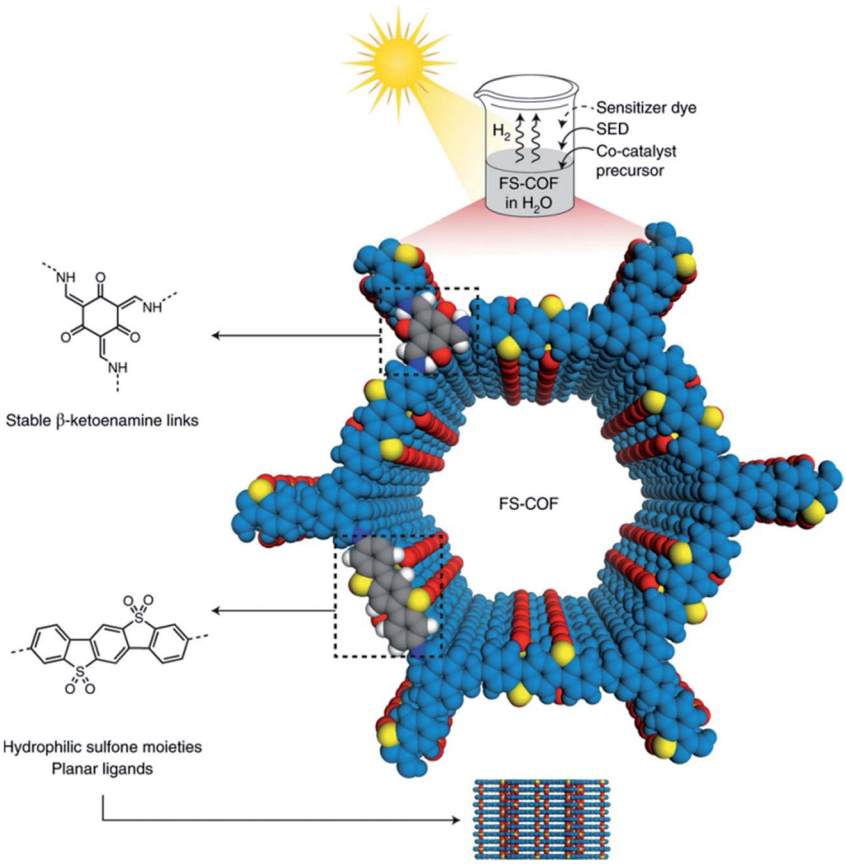

Fig. 5 Overview of the structural features of FS-COF for efficient photocatalytic hydrogen evolution. Reprinted from ref. 50 with the permission of Nature Publishing Group, Copyright 2018.

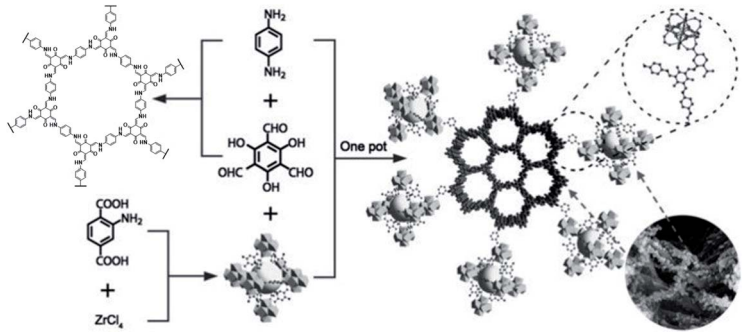

Fig. 6 Schematic representation of the preparation of NH_2-UiO-66/TpPa-1-COF hybrid materials. Reprinted with the permission of ref. 57. Copyright 2018, John Wiley and Sons.

lifetime. Second, the crystallinity and surface areas of the sulfone-functionalized COFs also increased, thereby improving the pore accessibility to the substrate molecules and highlighting the importance of crystallinity in the photocatalysis process. Third, the hydrophilicity or wettability due to the presence of sulfone groups is of significant importance for improved photocatalytic activity of such photoactive COF photocatalyst.[49]

The inherent porosity, crystallinity, chemical stability and structural tunability in combination with the tailorable semiconducting properties of COFs make them promising platforms to engineer efficient photoactive composites, therefore improving their photocatalytic activities. In 2014, Banerjee *et al.* employed TpPa-2-COF as a stable support matrix for anchoring CdS nanoparticles to form a CdS-COF composite and studied its photocatalytic properties towards hydrogen evolution. This

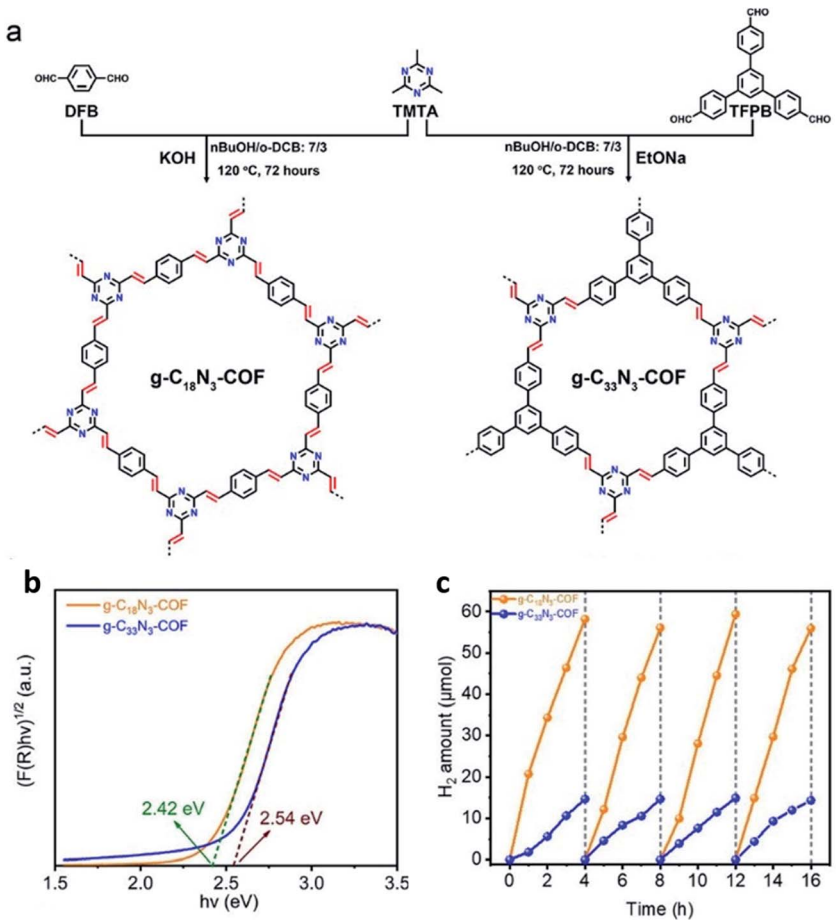

Fig. 7 (a) Schematic illustration of the synthesis of olefin-linked COFs. (b) Optical band gaps determined by the Tauc-plot method. (c) Photostability test of the studied COFs under visible-light irradiation (λ > 420 nm). Reproduced from ref. 59 with the permission of the American Chemical Society, Copyright 2019.

study demonstrated that effective assembly of organic and inorganic materials within a single hybrid commonly resulted in improved photocatalytic activity compared to that of each of the constituents.[51] Similarly, the Zhang group integrated TpPa-1-COF with MoS_2 to construct a MoS_2/TpPa-1-COF hybrid for boosting visible-light driven hydrogen evolution.[52] Recently, Zang and co-workers reported a novel Mo_3S_{13}@EB-COF composite by encapsulating anionic $[Mo_3S_{13}]^{2-}$ clusters in the cationic EB-COF and the obtained composite exhibited a remarkable HER of 13 125 μmol g^{-1} h^{-1} over 18 h under visible-light irradiation.[53] Graphitic carbon nitride (g-C_3N_4) has emerged as one of the most promising photocatalysts for visible-light driven hydrogen evolution.[54,55] In this context, Yan and co-workers for the first time synthesized a COF-modified g-C_3N_4 composite, termed as CN-COF, with imine linkage between them. Impressively, the resulting CN-COF hybrid showed a superior HER of 10.1 mmol g^{-1} h^{-1}, which is mainly attributed to the wide visible-light absorption and the efficient separation and migration of the photogenerated electron–hole pairs.[56] Very recently, Lan *et al.* successfully prepared a new type of MOF/COF composite by covalently anchoring different amounts of NH_2-UiO-66 onto the surface of TpPa-1-COF (Fig. 6). Owing to the matching of band gaps between TpPa-1-COF and NH_2-UiO-66, the obtained hybrid material exhibited efficient photocatalytic hydrogen evolution with a maximum HER of 23.41 mmol g^{-1} h^{-1} and a TOF of 402.36 h^{-1}, which was approximately 20-fold higher than that of the parent TpPa-1-COF, and outperformed all the reported MOF- and COF-based photocatalysts.[57]

In the literature, most of the reported COF-based photocatalysts are based on imine-, hydrazone- or azine-linked COFs; they are more or less not that stable for long-term photocatalysis in water and these linkages can only transmit partial π conjugation between building units and knots and limit their extension to full π conjugation. Very recently, Jiang *et al.* reported a fully π conjugated 2D sp^2 carbon COF for efficient photocatalytic hydrogen production from water. Notably, the resulting sp^2c-COF was exceptionally stable upon treatment for 7 days in organic solvents, water, 12 M HCl and 14 M NaOH aqueous solutions. The extended π conjugation not only improved the light absorbance but also promoted the exciton migration. As a result, the crystalline sp^2c-COF exhibited a steady HER of 1360 μmol g^{-1} h^{-1} without any decrease in activity over 5 h under visible-light irradiation ($\lambda \geq 420$ nm), while the amorphous sp^2c-CMP only gave a HER of 140 μmol g^{-1} h^{-1} under identical conditions.[58] Similarly, two semiconducting triazine-based sp^2c-COFs with unsubstituted olefin linkages were reported by the Zhang group (Fig. 7a). Their optical band gaps were calculated to be 2.42 and 2.54 eV for g-$C_{18}N_3$-COF and g-$C_{33}N_3$-COF, respectively (Fig. 7b). The

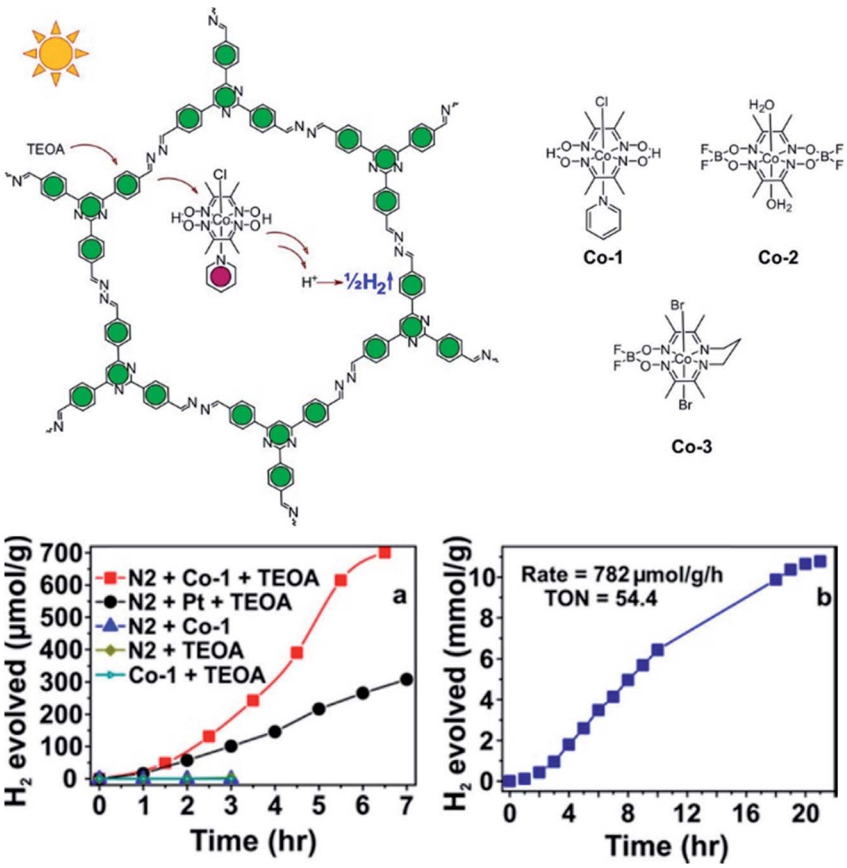

Fig. 8 Structures of the N_2-COF and the Co-catalysts and their photocatalytic hydrogen evolution performance under AM 1.5 light irradiation. Adapted with the permission of ref. 61. American Chemical Society, Copyright 2017.

photocurrent and EIS measurements confirmed the better performance of g-$C_{18}N_3$-COF than g-$C_{33}N_3$-COF; thus, g-$C_{18}N_3$-COF is expected to exhibit better photocatalytic activity. The average HER of g-$C_{18}N_3$-COF reached 292 μmol g^{-1} h^{-1}, which was nearly 4-fold that of g-$C_{33}N_3$-COF (74 μmol g^{-1} h^{-1}) under visible-light irradiation (Fig. 7c).[59] The same group also reported three other similar sp^2c-COFs *via* condensation of arylmethyl carbon atoms for photocatalytic hydrogen evolution, which exhibited relatively better hydrogen production activities than the above-mentioned COFs.[60]

Until now, most photocatalytic systems have incorporated the expensive noble platinum nanoparticles as the co-catalyst for hydrogen evolution, which seems to limit the development of environmentally benign photocatalytic hydrogen evolution systems. As such, the development of novel noble metal-free photocatalysts is of fundamental importance for sustainable and economical photocatalysis. In 2017, Lotsch *et al.* for the first time reported a noble metal-free photocatalytic system using azine-linked N_2-COF as the photoabsorber and chloro(pyridine)cobaloxime as the co-catalyst; a HER of 782 μmol g^{-1} h^{-1} and a turnover number (TON) of 54.4 were obtained in an acetonitrile/water mixture under AM 1.5 radiation (Fig. 8).[61] Subsequently, they employed a thiazolo[5,4-*d*] thiazole-linked COF (TpDTz) as the photoabsorber and the NiME cluster as the co-catalyst for sustained hydrogen evolution. Notably, a maximum rate of 941 μmol g^{-1} h^{-1} and a TON_{Ni} of 103 (70 h) were observed for the TpDTz-COF, surpassing those of many previously reported benchmark photocatalysts, and a specifically designed continuous-flow system for non-invasive monitoring of H_2 production was built to gather detailed insights into the reaction mechanism.[62]

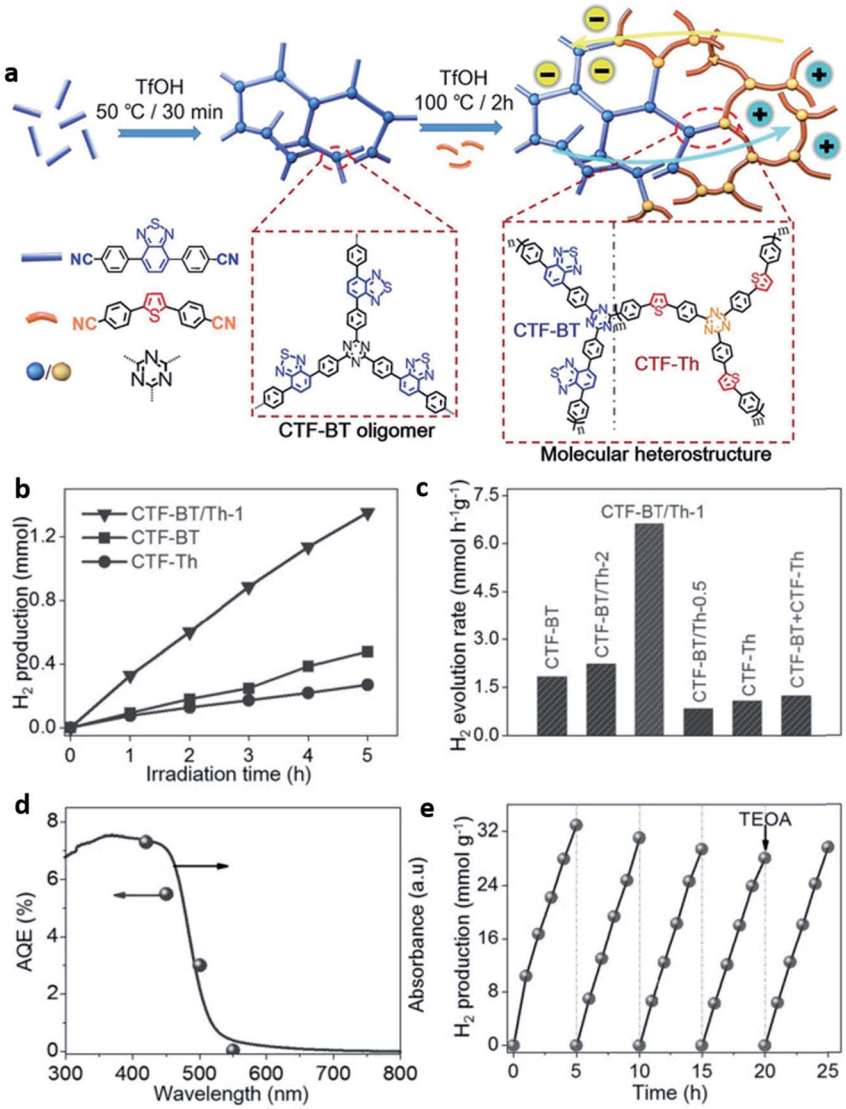

Fig. 9 (a) Schematic representation of the preparation of CTF-BT/Th. (b and c) Photocatalytic performance of the studied CTFs. (d) Wavelength-dependent AQE of CTF-BT/Th-1 and (e) photostability test of CTF-BT/Th-1. Adapted from ref. 71 with permission from John Wiley and Sons, Copyright 2019.

Along these lines, Sun and co-workers introduced $Ni(OH)_2$ into the TpPa-2-COF to afford a noble metal-free photocatalytic system for enhanced photocatalytic hydrogen evolution activity. The optimized HER for $Ni(OH)_2$-2.5%/TpPa-2-COF can reach up to 1896 μmol g^{-1} h^{-1}, 26.3 times higher than that of the pristine TpPa-2-COF.[63] To avoid the utilization of the precious Pt co-catalyst, Zhao *et al.* employed a newly designed NUS-55 COF as the platform to afford two cobalt-containing photocatalysts by post-modification of NUS-55 with $Co(NO_3)_2$ and $[Co\text{-}(bpy)_3]Cl_2$, respectively, which exhibited excellent photocatalytic hydrogen production activities.[64]

As a subclass of COFs, CTFs normally feature extremely high thermal and chemical stability as well as high nitrogen content, which have shown attractive photocatalytic properties under visible-light irradiation.[18] In 2015, Wu *et al.* for the first time employed CTFs as the photocatalyst for hydrogen evolution under visible-light irradiation. The studied CTF-T1 showed an optical band gap of 2.94 eV and a relatively low HER of 200 μmol g^{-1} h^{-1} in the presence of 3 wt% Pt as the co-catalyst.[65] Since then, numerous CTFs have been designed and studied for application in photocatalytic hydrogen evolution.[66–70] Heteroatom substitution on the backbones of CTFs is an effective approach to engineer and tune their optoelectronic properties. For example, Li and co-workers synthesized a set of molecular heterostructures, namely CTF-BT/Th-*x*, *via* a sequential polymerization strategy (Fig. 9a).[71] The resulting CTF materials exhibited much higher charge-carrier separation efficiency due to their staggered band gap alignment across the heterojunction. As a result, a remarkable HER of 6.6 mmol g^{-1} h^{-1} was obtained for CTF-BT-Th-1 under visible-light irradiation, which was 4- to 6-fold higher than those of single-component CTF-BT and CTF-Th (Fig. 9b and c). Moreover, the apparent quantum efficiency (AQE) of CTF-BT/Th-1 at 420 nm reached up to 7.3%, which was claimed to be the highest among all reported triazine-based photocatalysts (Fig. 9d). Besides its excellent activity, CTF-BT/Th-1 also exhibited impressive photostability (Fig. 9e). By tailoring the electron donors through substituting the heteroatoms (*e.g.* O, S and N) in the structure of CTFs, Tan *et al.* reported a series of CTFs and systematically examined their photocatalytic hydrogen evolution performance under visible-light irradiation. In line with the electron-donating ability and trend of the band gaps, the CTFs exhibited an enhanced HER from CTF-O (72 μmol g^{-1} h^{-1}) to CTF-N (538 μmol g^{-1} h^{-1}) under identical conditions.[70] Apart from the introduction of heteroatoms into CTFs *via* pre-designing various building blocks, heteroatom doping is another efficient approach to boost the photocatalytic performance of CTFs. Su *et al.* constructed a set of sulfur-doped CTFs by annealing treatment of CTFs with sulfur. The sulfur content in the framework was determined to be 0.5–0.52 atom% and the CTFS10 mixed with 10 wt% sulfur exhibited a maximum HER of 2000 μmol g^{-1} h^{-1}, which is 5 times higher than that of the pristine CTF material.[66] Similarly, improved photocatalytic hydrogen production activity of CTFs could also be achieved by doping phosphorus into CTF-1 because of the enhanced visible light absorption, increased reducing ability of photoelectrons and more efficient charge-carrier separation.[67]

Integration of electron-rich donor (D) and electron-deficient acceptor (A) building units in one specific structure is one of the most prevailing approaches in the field of polymers to improve their solar energy conversion.[18] Inspired by this approach, Jin *et al.* reported a set of D–A1–A2 type CTFs, in which triazine units (A1) and benzothiadiazole units (A2) serve as the acceptors and the carbazole unit acts as the donor. Interestingly, the photocatalytic hydrogen production activity of the CTFs can be readily tuned by varying the ratio of acceptor building units. As a result, a maximum HER of 19.3 mmol g^{-1} h^{-1} and an apparent quantum yield (AQY) of 22.8% at 420 nm were achieved in ter-CTF-0.7.[68]

To overcome the poor crystallinity of CTFs, Tan and co-workers constructed a set of crystalline CTFs (CTF-HUST-1 to CTF-HUST-4) *via* the low temperature condensation of aldehydes and amidines, which were further exploited as the photocatalysts for efficient hydrogen evolution. Compared with the CTFs prepared under conventional ionothermal conditions, the

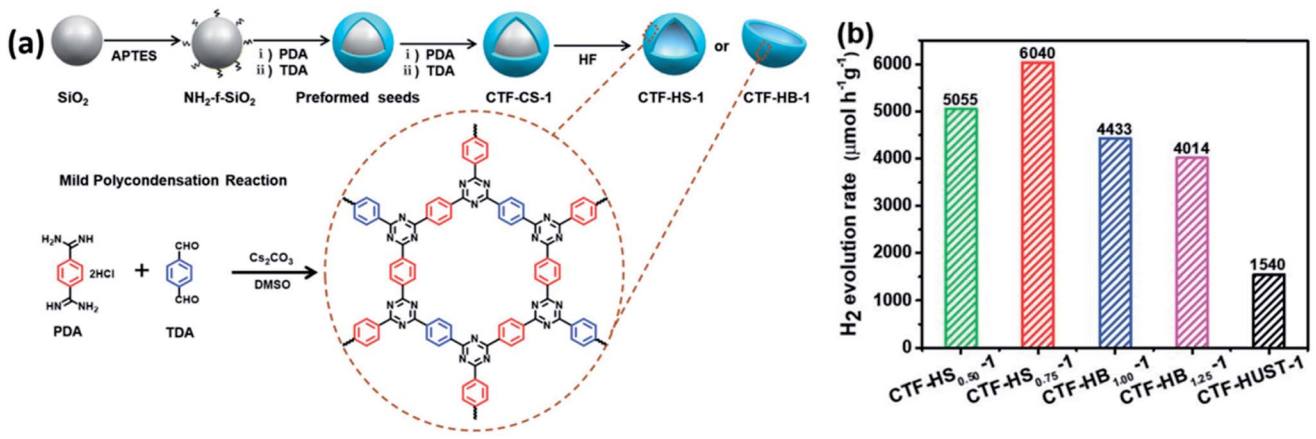

Fig. 10 (a) The schematic synthetic route of CTF-CS-1, where CS represents the NH_2-f-SiO_2@CTF-HUST-1 core–shell structure, HS is the hollow sphere morphology and HB is the hollow-bowl-like structure morphology. (b) HER of the studied hollow CTFs. Reprinted from ref. 72 with the permission of John Wiley and Sons, Copyright 2019.

Table 1 Summary of the representative COFs for photocatalytic hydrogen evolution under visible-light irradiation

COFs	Band gap (eV)	Co-catalyst	Sacrificial agent	HER (μmol g^{-1} h^{-1})	AQY (%)	Ref.
g-$C_{40}N_3$-COF	2.36	Pt	Na_2S	4	—	60
g-$C_{40}N_3$-COF	2.36	Pt	TEA	12	—	60
g-$C_{40}N_3$-COF	2.36	Pt	Na_2SO_3	14	—	60
N_0-COF	2.6–2.7	Pt	TEOA	23	0.0017 (500 nm)[c]	42
TpPa-2-COF	2.52	Pt	Lactic acid	28	—	51
g-$C_{40}N_3$-COF	2.36	Pt	EtOH	56	—	60
TpPa-2	2.07	Pt	Sodium ascorbate	72.09	—	63
BE-COF	2.12	Pt	Ascorbic acid	76.0	—	73
PTP-COF	2.1	Pt	TEOA	83.83	—	74
N_1-COF	2.6–2.7	Pt	TEOA	90	0.077 (450 nm)[c]	42
N_1-COF	—	Co-1	TEOA	100	—	61
CTP-1	2.96	Pt	TEOA	120	—	75
sp^2c-CMP	1.96	Pt	TEOA	140	—	58
TTR-COF	2.71	Au	TEOA	141	—	46
TTB-COF	2.8	Au	TEOA	145.25	—	46
N3-COF	—	Co-1	TEOA	163	—	61
OB-POP-1	2.21	Pt	TEOA	168	—	76
CTF-1	2.23	Pt	TEOA	168	—	77
B-CTF-1	2.14	Pt	TEOA	179	—	77
TpPa-COF-NO_2	1.92	Pt	Sodium ascorbate	220	—	44
COF-42	—	Co-1	TEOA	233	—	61
TP-BDDA	2.31	Pt	TEOA	324 ± 10	1.8 (520 nm)[d]	45
CTF-15	2.58	Pt	TEA	352	15.9 (420 nm)[e]	78
TBC-COF	—	Pt	TEOA	360	0.87 (420 nm)[d]	77
N_2-COF	—	Co-2[b]	TEOA	414	—	61
N_2-COF	2.6–2.7	Pt	TEOA	438	0.19 (450 nm)[c]	42
CTP_{300}	2.36	Pt	TEOA	500	2.4 (405 nm)	75
N_2-COF	—	Co-1[a]	TEOA	782	0.16[d]	61
OB-POP-2	2.28	Pt	TEOA	940	—	76
TpDTz COF	2.07	NiME	TEOA	941	0.2 (400 nm)[d]	62
CTF-1-10 min	2.26	Pt	TEOA	1072	9.2 (450 nm)[d]	79
CTF-Th	2.38	Pt	TEOA	1100	—	71
OB-POP-4	2.37	Pt	TEOA	1114	—	76
TpPa-1-COF	2.02	Pt	Sodium ascorbate	1223	—	57
OB-POP-3	2.14	Pt	TEOA	1322	2.0 (420 nm)	76
sp^2c-COF	1.9	Pt	TEOA	1360	—	58
CTF-O	2.67	Pt	TEOA	1440	2.10 (420 nm)	70
CTF-HUST-1	2.03	Pt	TEOA	1540	—	72
TpPa-COF	2.09	Pt	Sodium ascorbate	1560	—	44
TP-COF	2.28	Pt	Ascorbic acid	1600 (±80)	—	49
N_3-COF	2.6–2.7	Pt	TEOA	1703	0.44 (450 nm)[c]	42
CTF-BT	2.51	Pt	TEOA	1800	—	71
$Ni(OH)_2$–2.5%/TpPa-2	—	$Ni(OH)_2$	Sodium ascorbate	1895.99	—	63
TFPT-COF	2.8	Pt	TEOA	1970	2.2 (400 nm)[f]	35
$CTFS_{10}$	1.87	Pt	TEOA	2000	—	66
sp^2c-COF_{ERDN}	1.85	Pt	TEOA	2120	0.48 (495 nm)	58
g-$C_{40}N_3$-COF	2.36	Pt	TEOA	2596	4.84(±0.27) (420 nm)	60
TpPa-COF-CH_3	2.10	Pt	Sodium ascorbate	3070	—	44
CdS-COF(90 : 10)	—	Pt	Lactic acid	3678	4.2 (420 nm)	51
S-COF	2.10	Pt	Ascorbic acid	4440 (±140)	—	49
CTF-S	2.47	Pt	TEOA	5320	4.11 (420 nm)	70
TpPa-1	2.11	Pt	Ascorbic acid	5479	—	52
MoS2-3%/TpPa-1-COF	2.14	MoS_2	Ascorbic acid	5585	0.76 (420 nm)[d]	52
CTF-$HS_{0.75}$–1	2.70	Pt	TEOA	6040	4.2 (420 nm)	72
CTF-BT/Th-1	2.51	Pt	TEOA	6606	7.3(420 nm)[d]	71
CTF-$HS_{0.75}$–2	—	Pt	TEOA	7100	6.8 (420 nm)	72
TpPa-COF-$(CH_3)_2$	2.06	Pt	Sodium ascorbate	8330	—	44
TP-COF	1.97	PVP-Pt	Ascorbic acid	8420	0.4 (475 nm)[d]	73
CTF-CBZ	2.17	Pt	TEOA	9920	4.07 (420 nm)	68
CN-COF	2.09	Pt	TEOA	10 100	20.7 (425 nm)[d]	56
Pd^0/TpPa-1-EosinY	—	—	TEOA	10 400	—	80
CTF-N	2.17	Pt	TEOA	10 760	4.07 (420 nm)	70
20%CdS-CTF-1	—	Pt	Lactic acid	11 430	16.3 (420 nm)	81

Table 1 (*Contd.*)

COFs	Band gap (eV)	Co-catalyst	Sacrificial agent	HER (μmol g^{-1} h^{-1})	AQY (%)	Ref.
CdS NPs/3%CTF-1	2.36	Pt	Lactic acid	12 150	—	82
Mo_3S_{13}@EB-COF	—	$Ru(bpy)_3Cl_2$	Ascorbic acid	13 215	4.49 (475 nm)[d]	53
ter-CTF-0.7	2.11	Pt	TEOA	19 320	22.8 (420 nm)	68
NH_2-UiO-66/TpPa-1-COF(4 : 6)	2.10	Pt	Sodium ascorbate	23 413	—	57
FS-COF	1.85	Pt	Ascorbic acid	10 100 (±300)	3.2 (600 nm)[e]	49
FS-COF + WS5F	—	Pt	Ascorbic acid	16 300 (±290)	2.2 (600 nm)[e]	49

[a] Co-1: [Co(dmgH)$_2$pyCl]. [b] Co-2: [Co(dmgBF$_2$)$_2$(OH$_2$)$_2$] [c] PE: photonic efficiency. [d] AQE: apparent quantum efficiency. [e] EQE: external quantum efficiency. [f] QE: quantum efficiency; TEOA: triethanolamine; TEA: triethylamine.

CTF-HUSTs exhibited much higher HERs, and CTF-HUST-2 showed a maximum HER of 2647 μmol g^{-1} h^{-1} under visible-light irradiation (λ > 420 nm) in the presence of a sacrificial agent and Pt co-catalyst.[32] Similarly, in one recent contribution, they synthesized a new type of hollow-structured CTF by the aforementioned polycondensation reaction *via* a template approach (Fig. 10a). Interestingly, the morphology of the CTFs can be tuned from a sphere to a bowl with the decrease of the shell thicknesses, and more importantly, the HER of the hollow-structured CTF (CTF-HS$_{0.75}$-1) can reach 6040 μmol g^{-1} h^{-1}, which was 4-fold that of the bulk CTF-HUST-1 (1540 μmol g^{-1} h^{-1}) under the same conditions (Fig. 10b).[72] Recently, the same group developed another strategy to construct crystalline CTFs by *in situ* controlled oxidation of alcohols to aldehyde monomers.[32] The decreased nucleation rate and generated lower nuclei concentration were thought to be the key factors affecting the crystallization process. Among all the obtained crystalline CTFs, CTF-HUST-C1 exhibited the highest HER of 5100 μmol g^{-1} h^{-1} under visible-light irradiation in the presence of 3 wt% Pt and 10% TEOA solution, which was much higher than that previously reported for CTF-HUST-1 (1460 μmol g^{-1} h^{-1}) and other amorphous CTFs.

To provide a better understanding and direct comparison of the photocatalytic hydrogen evolution activities of the previously reported COF-based photocatalysts, a detailed overview and summary of the representative photoactive COFs for photocatalytic hydrogen production under visible-light irradiation are listed in Table 1.

3.2. COFs for photocatalytic CO_2 reduction

Photocatalytic reduction of CO_2 into hydrocarbon fuels is a challenging yet promising approach for achieving a more sustainable alternative to conventional fossil fuels. Generally, the concept of photocatalytic reduction of CO_2 dates back to the 1970s, when Honda and co-workers firstly reported the photocatalytic reduction of CO_2 on various photosensitive semiconductor powders.[9] Since then tremendous efforts have been directed towards photocatalytic CO_2 reduction into valuable chemicals and solar fuels using diverse inorganic and organic photocatalysts.[2,3,83–86] COFs represent a class of advanced crystalline porous materials with structural tunability and diversity as well as high physiochemical stability, and some COFs with intriguing semiconducting properties and charge separation capabilities have been reported and developed for artificial photocatalysis. However, research on photocatalytic CO_2 reduction over COFs is still in its infancy.

In 2016, J.-O. Baeg *et al.* synthesized a triazine-based covalent organic framework (2D-CTF) film and evaluated its photocatalytic CO_2 reduction activity to form formic acid for the first time. The formic acid formation rate for the photocatalyst reached 881.3 μmol g^{-1} h^{-1}, making it a benchmark example of COFs for photocatalytic CO_2 reduction at that time.[87] Subsequently, Zhu and co-workers reported two azine-linked 2D COFs (ACOF-1 and N_3-COF), which were further applied as photocatalysts for photocatalytic reduction of CO_2 to methanol in the presence of H_2O under visible-light irradiation without any sacrificial agents (Fig. 11a). The amount of methanol formed over N_3-COF was 13.7 μmol g^{-1} in 24 h, higher than that of ACOF-1 (8.6 μmol g^{-1}) and g-C_3N_4 (4.8 μmol g^{-1}) (Fig. 11b). The density functional theory (DFT) calculation results confirmed that the electronic distribution of the HOMO and LUMO of N_3-COF was well separated, which was favorable for intramolecular charge transfer. Although the photocatalytic performance of the studied COFs was relatively poor, this study highlights the great potential and possibility of COFs as photocatalysts for photocatalytic CO_2 reduction.[88]

Homogeneous photocatalysts based on rhenium bipyridine (bpy) complexes have been extensively studied as molecular photocatalysts for various photocatalytic reactions and these types of photocatalysts often exhibited remarkable photocatalytic activities.[89,90] However, it is difficult to recover and reuse them for multiple cycles. In contrast, molecular active sites anchored on porous materials as heterogeneous catalysts can overcome this drawback and are expected to achieve better photocatalytic performance.[85,91] Cao and coworkers employed a pyridine-based CTF material as a platform to anchor the Re(CO)$_3$Cl complex, which was further evaluated as a photocatalyst for photocatalytic reduction of CO_2 to CO. The obtained Re-CTF-py photocatalyst exhibited the highest CO evolution rate of 353 μmol g^{-1} h^{-1} with a TON of 4.8 over 10 h under full light irradiation; this work highlighted the great potential of CTF materials as high-performance platforms to anchor single active sites for heterogeneous photocatalysis and explored the possibility and development of COFs for

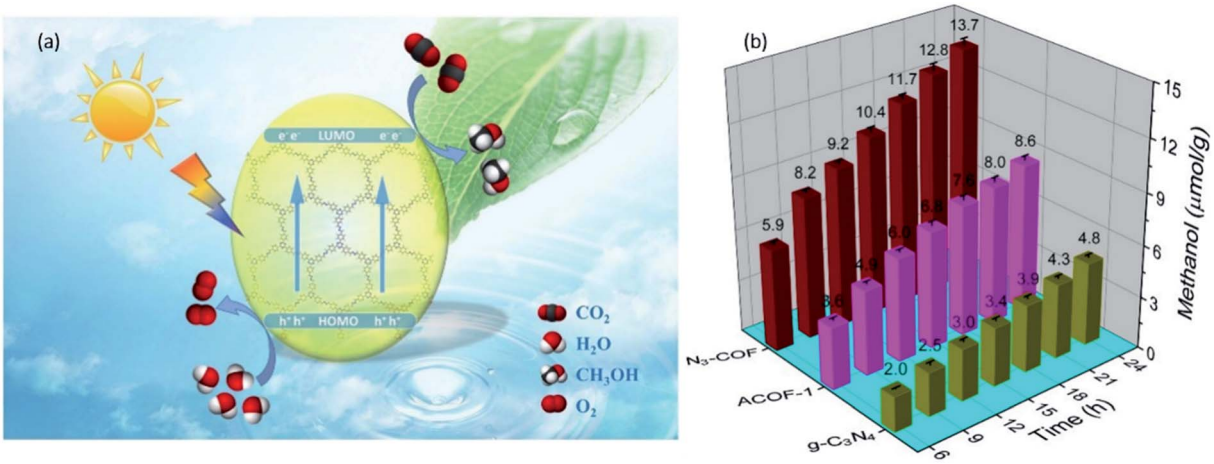

Fig. 11 (a) Schematic illustration for the photocatalytic reduction of CO_2 to CH_3OH over azine-based COFs. (b) Comparison of the amount of CH_3OH produced using ACOF-1, N_3-COF and g-C_3N_4 as the photocatalysts. Adapted with permission from ref. 88. Copyright 2018, Elsevier B.V.

photocatalytic CO_2 reduction.[92] Similarly, in 2018, Huang and coworkers reported an effective photocatalyst with a newly designed photoactive triazine-based COF as the photosensitizer and incorporated $Re(bpy)(CO)_3Cl$ as a CO_2 reduction molecular catalyst for visible light-driven CO_2 reduction (Fig. 12a–d). Under optimized conditions, the resulting Re-COF can steadily produce ~15 mmol CO br per g of Re-COF for 20 h after a 15 min induction period in acetonitrile solution with triethanolamine (TEOA) as a sacrificial reducing agent, accounting for a TON of 48 and 22-fold better activity than its homogeneous counterpart (Fig. 12e), which was mainly attributed to the efficient electron transfer from COFs to $Re(bpy)(CO)_3Cl$ and inhibited or retarded charge recombination in the Re-COF.[93] Along these lines, Cooper and coworkers recently anchored the $Re(bpy)(CO)_3Cl$ complex into a newly designed Bpy-sp^{2}c-COF to afford an efficient photocatalyst of Re-Bpy-sp^{2}c-COF with superior chemical stability, broad light absorption and strong CO_2 binding affinity, thus

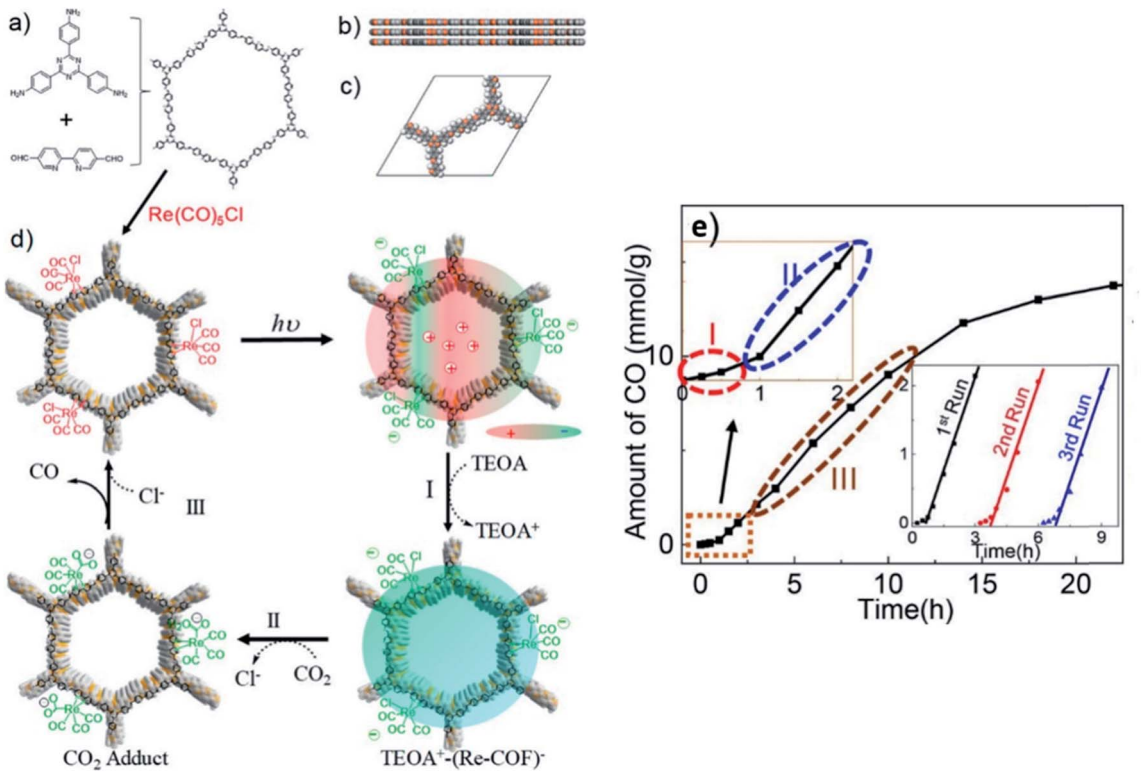

Fig. 12 (a) Synthesis of COF and Re-COF. (b) Side view and (c) unit cell of AA stacked COF. (d) Proposed catalytic mechanism for CO_2 reduction. (e) Amount of CO produced as a function of time. Adapted with the permission of ref. 93. Copyright 2018, American Chemical Society.

resulting in a maximum CO production rate of 1040 μmol g^{-1} h^{-1} with 81% selectivity over H_2 and its performance can even be enhanced to 1400 μmol g^{-1} h^{-1} of CO production with a CO/H_2 selectivity of 86% after dye-sensitization.[94] Recently, another rhenium-functionalized COF (Re-TpBpy) was developed to act as a recyclable photocatalyst for photocatalytic reduction of CO_2 to CO and the resulting Re-TpBpy exhibited twofold higher activity than the homogeneous complex under identical conditions. The minor deactivation of the Re-TpBpy over multiple tests was attributed to many factors, such as a leaching or poisoning of some Re active sites by the byproduct of the electron donor oxidation during the reaction.[95]

To achieve better photocatalytic performance towards CO_2 reduction, Jiang *et al.* recently synthesized a set of ultrathin (<2.1 nm) imine-linked COF nanosheets *via* a general bottom-up approach (Fig. 13a). Scanning tunneling microscopy (STM) clearly visualized the pore channels and the corresponding building blocks of the COF nanosheets (Fig. 13b). More importantly, the resulting COF-367-Co nanosheets exhibited impressive photocatalytic CO_2 to CO reduction activity with a maximum CO production rate of 10 162 μmol g^{-1} h^{-1} and a high CO selectivity of 78% over H_2 under visible-light irradiation (Fig. 13c). In contrast, a low CO production rate of 124 μmol g^{-1} h^{-1} and CO/H_2 selectivity of 13% were obtained by the bulk COF-367-Co under identical conditions.[96]

In recent years, other earth-abundant transition metal complexes with tunable activities and redox valences, including molecular cobalt and nickel complexes, have been widely studied for photocatalytic reduction of CO_2 in homogeneous systems.[97] Zou and co-workers designed a synergistic photocatalyst for selective photocatalytic reduction of CO_2 to CO by using a pyridine-based COF bearing single Ni sites (Ni-TpBpy), in which electrons transferred from the photosensitizer to Ni sites for CO evolution under visible-light irradiation (Fig. 14a). Remarkably, the obtained Ni-TpBpy photocatalyst exhibited an excellent activity of 4057 μmol g^{-1} for CO production in a 5 h reaction with a 96% CO selectivity over H_2 and superior photostability over 3 cycles (Fig. 14b–e). Theoretical calculations explicitly elucidated that single Ni sites in TpBpy undoubtedly served as the photocatalytically active sites, where CO_2 molecules were coordinated, activated, and reduced, and TpBpy not only served as a host for CO_2 molecules and single Ni sites but also inhibited the competitive H_2 evolution (Fig. 14f). Moreover, a possible reaction mechanism for the photocatalytic CO_2 reduction over Ni-TpBpy is proposed (Fig. 14g)[98] and this work highlights the great potential of COFs for photocatalytic applications through delicate design of their coordination environments around the catalytically active sites.

Similarly, Wu *et al.* reported a set of cobalt modified CTFs (Co/CTF-1) with different amounts of cobalt species prepared by a simple impregnation approach. Impressively, the obtained Co/CTF-1 exhibited 44-fold enhancement of its photocatalytic CO production rate over the pristine CTF-1; the CTF not only acted as a host for active Co species, but also bridged the photosensitizer with the active sites for efficient electron/hole

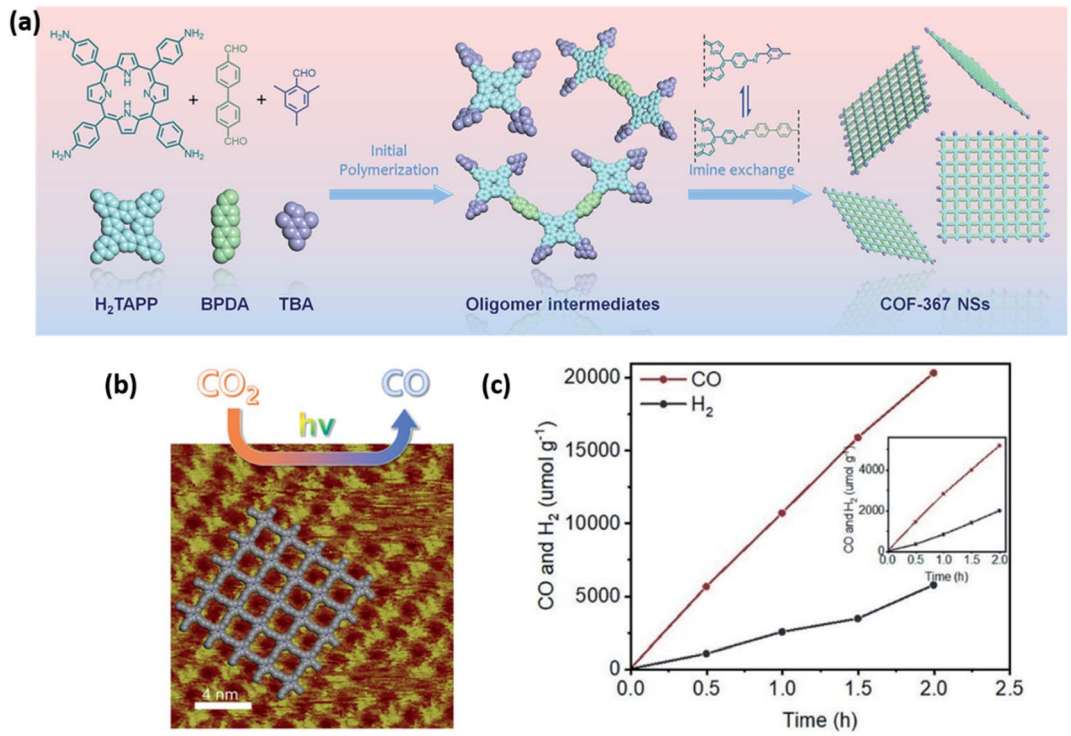

Fig. 13 (a) Schematic representation of the synthesis of COF-367 nanosheets. (b) STM image of COF-367 nanosheets. (c) Photocatalytic CO_2 reduction with time over COF-367-Co nanosheets under visible-light irradiation. Reproduced with the permission of ref. 96. American Chemical Society, Copyright 2019.

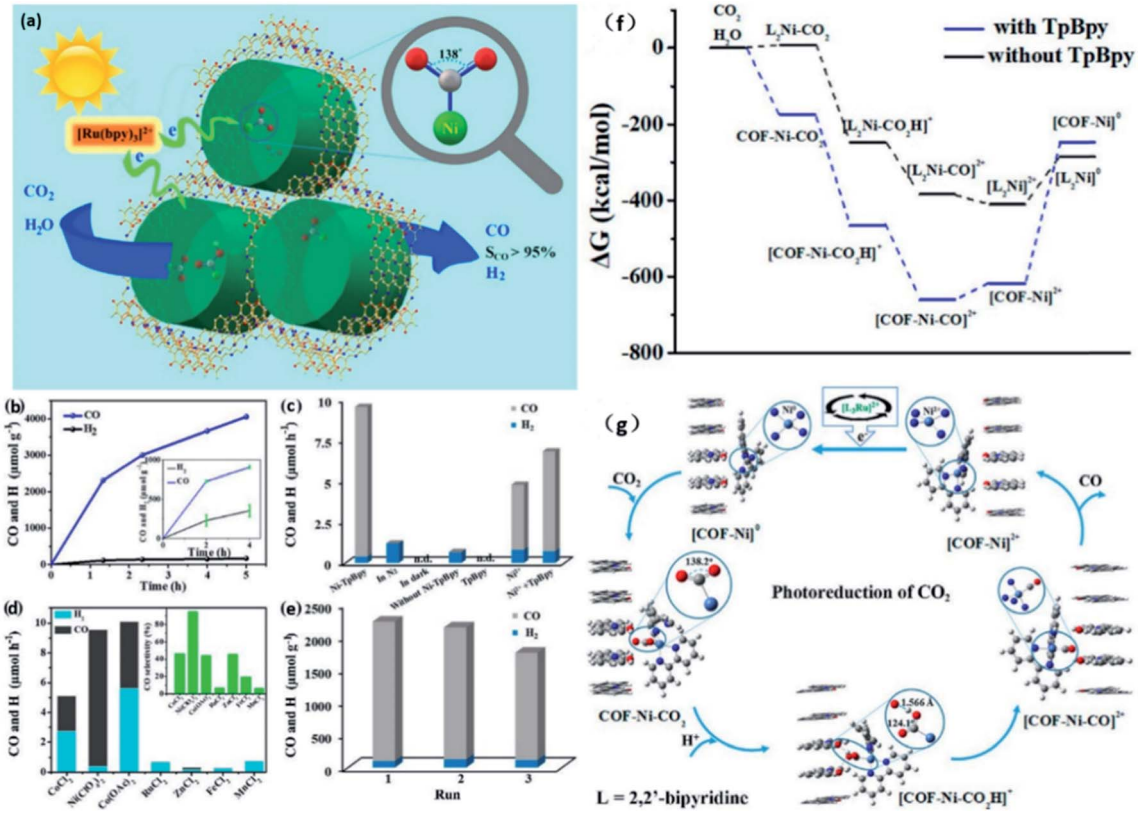

Fig. 14 (a) Schematic illustration of the photocatalytic CO_2 reduction over Ni-TpBpy. (b) Photocatalytic CO and H_2 evolution by Ni-TpBpy under 1 and 0.1 bar (diluted with argon, inset). (c) The study of different reaction conditions in a 2 h reaction. (d) Different metal ions anchored in TpBpy for CO_2 reduction in a 2 h reaction. (e) Photostability tests of Ni-TpBpy. (f) DFT-calculated relative Gibbs free energy (ΔG, kcal mol^{-1}) profiles with and without the optimized building block of TpBpy. (g) Proposed reaction mechanism for the photocatalytic conversion of CO_2 into CO on Ni-TpBpy. Reproduced with the permission of ref. 98. Copyright 2019, American Chemical Society.

pair transfer.[99] Recently, Lan and co-workers reported a series of transition metal ion modified COFs (DQTP COF-M, M = Co, Ni, Zn) for photocatalytic CO_2 reduction. Experimental results revealed that different transition metal species on COFs had great effects on their activity and selectivity of CO_2 reduction. Among all the obtained materials, DQTP COF-Co and DQTP

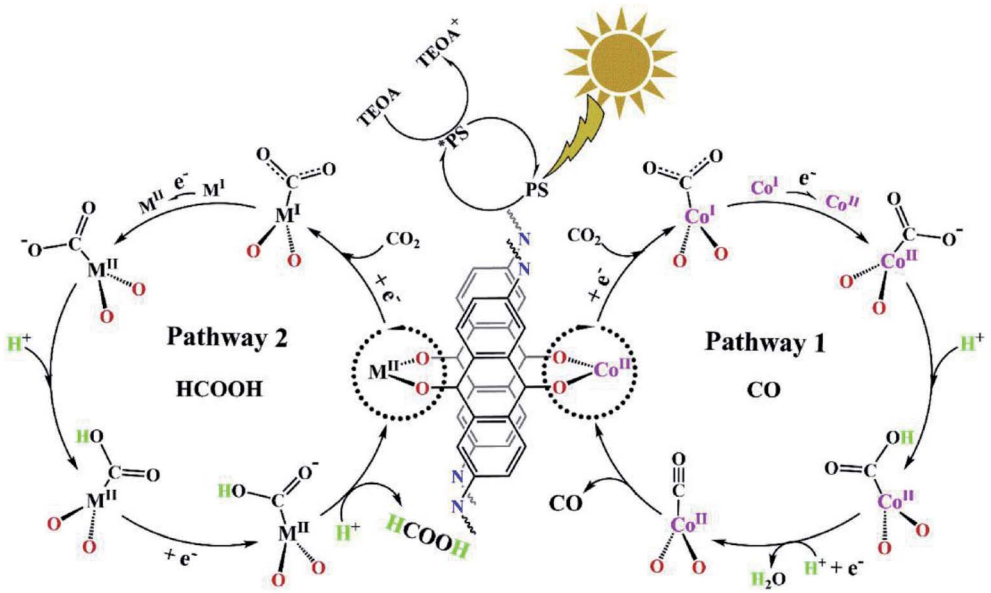

Fig. 15 Proposed mechanism of the photocatalytic CO_2 reduction over DQTP COF-M. Reprinted with permission.[100] Copyright 2019, Elsevier B.V.

COF-Zn exhibited the best CO and formic acid evolution rate of 1020 μmol g^{-1} h^{-1} and 152.5 μmol g^{-1} h^{-1}, respectively. Meanwhile, a "two-pathway" mechanism for photocatalytic CO_2 reduction over the studied COFs was proposed; selective evolution of CO or formic acid mainly depended on the environment of the metal ions: an electron-rich coordination environment tended to weaken and break the C–O bond in the metal –COOH intermediate to form CO, while an electron-deficient coordination environment could enhance the C–O bond force to form HCOOH (Fig. 15).[100]

Subsequently, the same group designed a set of porphyrin–tetrathiafulvalene-based COFs (TTCOF-M, M = 2H, Zn, Ni, Cu) for photocatalytic reduction of CO_2 in the presence of H_2O without additional photosensitizers, sacrificial agents and noble metal co-catalysts. The semiconducting properties of all the studied TTCOFs were determined by UV-Vis measurements and TTCOF-Zn gave an optical band gap of 1.49 eV (Fig. 16a). The detailed HOMO–LUMO energy alignments are shown in Fig. 16b. Among all the resulting TTCOFs, TTCOF-Zn exhibited the highest CO production rate of 2.06 μmol g^{-1} h^{-1} with approximately 100% selectivity and superior recyclability. The proposed mechanism is as follows: photoinduced electron transfer (PET) occurs from the electron-rich TTF moiety (HOMO center) to the electron-deficient TAPP moiety (LUMO center) after absorption of photons under visible light irradiation; then, the excited electrons move to the catalytically active sites (Zn or Cu in TAPP) and are used for photocatalytic CO_2 reduction. Meanwhile, the photogenerated holes in TTF are able to oxidize H_2O to O_2 to make sure that the catalytic system gains electrons from H_2O to balance the charge (Fig. 16c and d).[101]

Although the study of COFs for photocatalytic CO_2 reduction in the literature is still in its infancy (Table 2), it has shown great promise and we can expect that there will be more and more research focusing on the development of more efficient and promising COF-based photocatalysts for the utilization of CO_2.

3.3. COFs for photoredox reactions

In the field of homogeneous catalysis, numerous transition metal complexes and organic dyes have been used as efficient

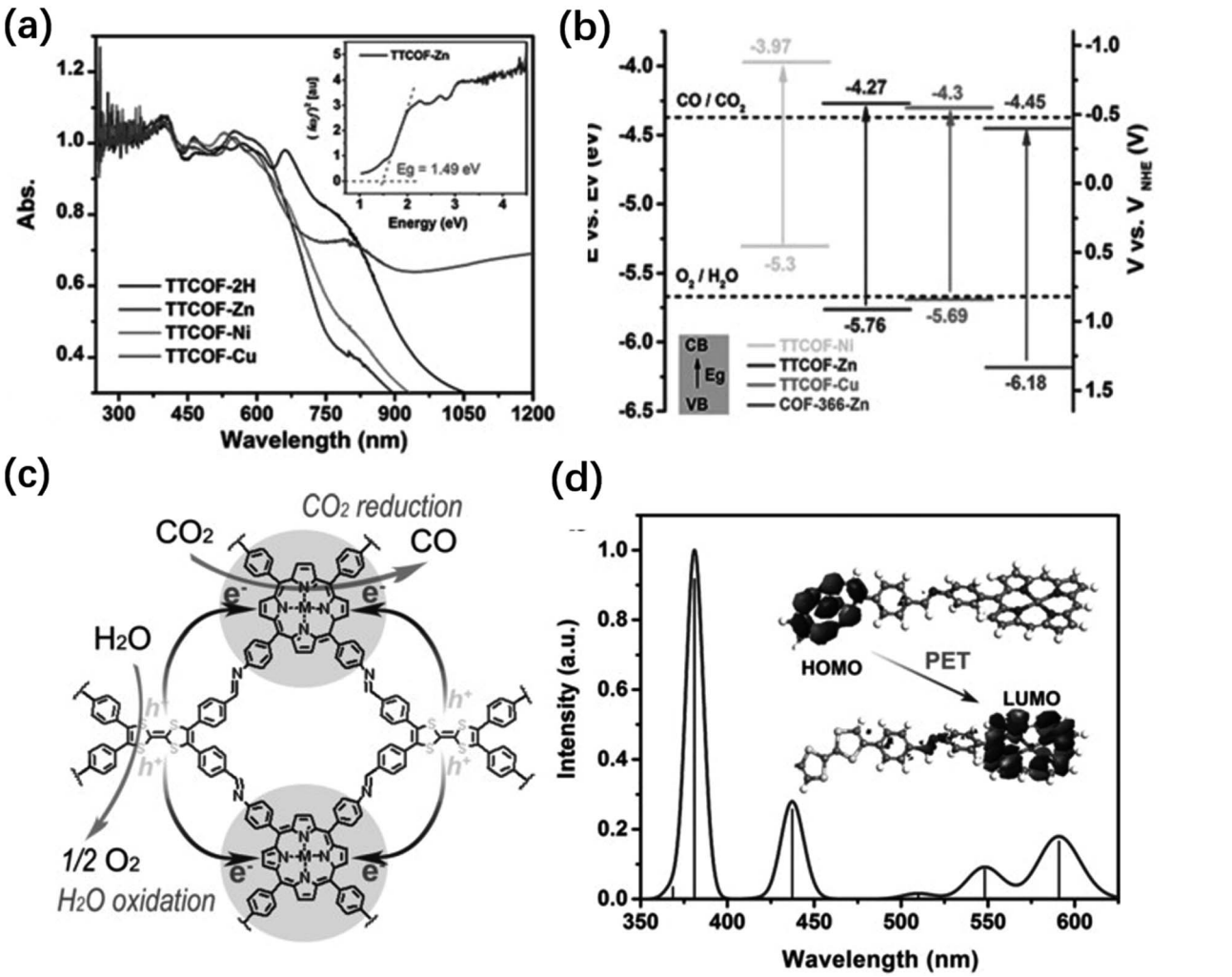

Fig. 16 (a) Solid-state UV/Vis spectra of TTCOF-M. (b) Band structure diagram for TTCOF-M and COF-366-Zn. (c) Schematic illustration of the proposed mechanism of TTCOF-M for photocatalytic CO_2 reduction with H_2O. (d) Theoretical UV-Vis simulation of TTCOF-Zn and scheme of the PET route under light irradiation. Reprinted with the permission of ref. 101. Copyright 2019, John Wiley and Sons.

Table 2 Summary of the performance of some representative COFs for photocatalytic CO_2 reduction

COFs	Band gaps (eV)	Light source	Products	Ref.
2D-CTF film	2.05	450 W Xe lamp ($\lambda > 420$ nm)	881.3 μmol g^{-1} h^{-1} of HCOOH	87
ACOF-1	2.69	500 W Xe lamp (420 nm < λ < 800 nm)	8.6 μmol g^{-1} of CH_3OH in 24 h	88
N_3-COF	2.57	500 W Xe lamp (420 nm < λ < 800 nm)	13.7 μmol g^{-1} of CH_3OH in 24 h	88
Re-CTF-py	—	300 W Xe lamp (200 nm < λ < 1100 nm)	353.05 μmol g^{-1} h^{-1} of CO within 10 h	92
CTF-py	—	300 W Xe lamp (200 nm < λ < 1100 nm)	13.4 μmol g^{-1} h^{-1} of CO within 10 h	92
Re-COF	—	225 W Xe lamp ($\lambda > 420$ nm)	15 mmol g^{-1} of CO with 98% selectivity for 20 h	93
Re-Bpy-sp^2c-COF	—	300 W Xe lamp ($\lambda > 420$ nm)	1040 μmol g^{-1} h^{-1} of CO with 81% selectivity	94
Re-Bpy-sp^2c-COF-dye	—	300 W Xe lamp ($\lambda > 420$ nm)	1400 μmol g^{-1} h^{-1} of CO with 86% selectivity	94
Re-TpBpy	—	200 W Xe lamp ($\lambda > 390$ nm)	~3.2 mmol g^{-1} h^{-1} of CO in 12 h for the 1st run	95
COF-367-CoNSs	—	300 W Xe lamp ($\lambda > 420$ nm)	10.162 mmol g^{-1} h^{-1} of CO with 78% selectivity	96
Ni-TpBpy	2.03	300 W Xe lamp ($\lambda > 420$ nm)	4057 μmol g^{-1} of CO with 96% selectivity in 5 h	98
Co/CTFs	—	300 W Xe lamp ($\lambda > 420$ nm)	50 μmol g^{-1} h^{-1} of CO in 4 h	99
DQTP COF-Co	1.55	300 W Xe lamp ($\lambda > 420$ nm)	1020 μmol g^{-1} h^{-1} of CO	100
DQTP COF-Zn	1.61	300 W Xe lamp ($\lambda > 420$ nm)	152.5 μmol g^{-1} h^{-1} of HCOOH with 90% selectivity	100
TTCOF-Zn	1.49	300 W Xe lamp ($\lambda > 420$ nm)	12.33 μmol of CO with 100% selectivity	101

photocatalysts for various photoredox reactions; however, their homogeneous nature and the associated limitations, such as recovery difficulty, high cost and poor recyclability, significantly limit their large-scale and widespread applications. Owing to the tunable optoelectronic properties and high crystallinity and stability, COFs have been effectively employed as promising photocatalysts or designer platforms for various photocatalytic organic transformation reactions in recent years.

Aromatic aldehydes are indispensable compounds and play an important role in the chemical and medical industries. Among all the methods, photocatalytic oxidation of alcohols to aldehydes with various photocatalysts is regarded as an environmentally benign technique and has received great attention in recent years. Wang *et al.* constructed a range of NH_2-MIL-125@TAPB-PDA-COF hybrid materials with different thicknesses of COF shells *via* a facile seed growth approach, which were further employed as photocatalysts for the photocatalytic oxidation of benzyl alcohol. Especially, the composite with a COF shell thickness of around 20 nm exhibited a benzaldehyde yield of 94.7%, which was 2.5-fold and 15.5-fold that of the pristine NH_2-MIL-125 and TAPB-PDA-COF and this composite also exhibited excellent activity and stability towards various substituted alcohols. The superior photocatalytic performance of the hybrid was mainly attributed to the enhanced light absorption ability and separation and migration of the photoexcited electron–hole pairs between the MOF and COF interfaces.[102] Along these lines, the same group reported another type of core–shell hybrid photocatalyst by encapsulation of TiO_2 nanobelts into an imine-linked PAPB-PDA-COF for photocatalytic oxidation of aromatic alcohols. Impressively, the composite gave a maximum benzyl alcohol conversion of 92.5%, which was much higher than that of TiO_2 (9.2%) and PAPB-PDA-COF (7.2%) under identical conditions.[103]

Phenols, as important intermediates for the preparation of polymers and pharmaceutical medicines, can be facilely synthesized through oxidative hydroxylation of arylboronic acids.[104] The Wang group developed a "killing two birds with one stone" strategy to obtain three ultrastable benzoxazole-linked COFs, which were used as metal-free photocatalysts for photocatalytic oxidative hydroxylation of arylboronic acids to phenols (Fig. 17a). The transformation of 4-carboxyphenylboronic acid to 4-hydroxybenzoic acid was initially selected as the model reaction. Impressively, LZU-190 exhibited superior and unchanged activity (99% yield) even after 20 cycles with iPr2Net as the sacrificial agent in air. More importantly, the universality of LZU-190 as an efficient photocatalyst was further confirmed by photocatalytic reactions of a set of arylboronic acids bearing different electron-withdrawing or electron-rich substituents.

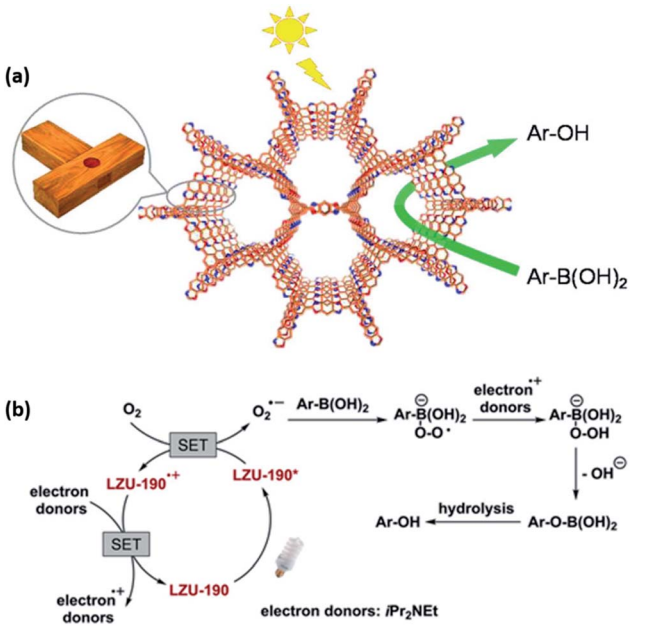

Fig. 17 (a) Schematic illustration of the photocatalytic oxidative hydroxylation of arylboronic acids to phenols. (b) Proposed mechanism for the photocatalytic oxidative hydroxylation of arylboronic acids to phenols with LZU-190 as the photocatalyst. Reprinted from ref. 105 with the permission of the American Chemical Society, Copyright 2018.

The proposed mechanism for this reaction is the generation of excited LZU-190* *via* visible-light irradiation, and then superoxide radical anions ($O_2^{\bullet -}$) were formed *via* single electron transfer (SET) from LZU-190* to O_2, which further added to the arylboronic acids to generate intermediate A and intermediate A further extracted a hydrogen atom from the electron donor to form intermediate B. Then, intermediate B was rearranged with the loss of $-OH^-$ to give C and intermediate C was subsequently hydrolyzed to afford the phenols (Fig. 17b).[105] Recently, Chen and co-workers studied the same reaction by employing an ultrastable imine-based BBO-COF as the photocatalyst, which was synthesized by self-polycondensation of an A2B2 building block and exhibited excellent photoactivity and recyclability towards a wide range of substrates.[106]

Another important oxidation reaction is the oxidation of sulfides to sulfoxides, which are key intermediates in the pharmaceutical and agrochemical industries.[4,104] Wang *et al.* designed and synthesized two porphyrinic COFs, named 2D-PdPor-COF and 3D-PdPor-COF, respectively (Fig. 18a). To study the influence of dimensionality on COF functionality, they investigated the photocatalytic activities of both COFs towards oxidation of thioanisole to methyl phenyl sulfoxide. Interestingly, a yield of 98% in 0.4 h was obtained for 3D-PdPor-COF, while the yield was only 48% under identical conditions for 2D-PdPor-COF. More importantly, the 3D-PdPor-COF exhibited certain size-selective photocatalysis towards different substrates with diverse substituents and sizes (Fig. 18b).[107]

Cabrera and co-workers employed a set of imine-linked COFs with different morphologies as the photocatalysts for photocatalytic sulfoxidation reactions. The crystalline laminar material, namely COF-1b, displayed significantly high yields of sulfoxide for a large variety of substrates under visible light irradiation with ethanol/water as the solvent and the photocatalyst can be reused for at least 9 cycles without a significant decrease of its activity.[108]

Besides photooxidation reactions, photocatalytic reductive reactions are also of great importance in the field of organic synthesis. Liu *et al.* reported a newly designed D–A type imine-linked photoactive COF (COF-JLU22) for reductive dehalogenation of phenacyl bromide derivatives under visible-light irradiation (Fig. 19a). The integration of electron donor and acceptor units in the π-conjugated layers leads to the superior light absorption ability and sensitive photoelectric response character of the COF-JLU22 material. As a result, COF-JLU22 exhibited remarkable photoreductive dehalogenation activity of up to 99% yield towards various derivatives of phenacyl bromide with different electron-deficient and electron-rich substituents and it can be efficiently reused for at least 5 cycles with negligible loss of its photocatalytic activity (Fig. 19b). Based on the experimental results, a plausible mechanism for this reaction was proposed by the authors (Fig. 19c).[109]

Previous studies have revealed the superior properties of core–shell structures for various applications.[110] Motivated by the advantages of core–shell hybrids, Zhang *et al.* reported a hollow nanoporous CTF material *via* a trifluoromethanesulfonic acid vapor-assisted method with SiO_2 nanoparticles as the template for photocatalytic reduction of 4-nitrophenol (4-NP) to 4-aminophenol (4-AP). Interestingly, the reduction of 4-NP was completed in 50 min with an average TOF of 0.18 h^{-1} for hollow CTF-BT, while the conversion is only 46% with a TOF of 0.08 h^{-1} for the bulk CTF-BT, indicating the importance of the hollow structure.[111] Similarly, a palladium

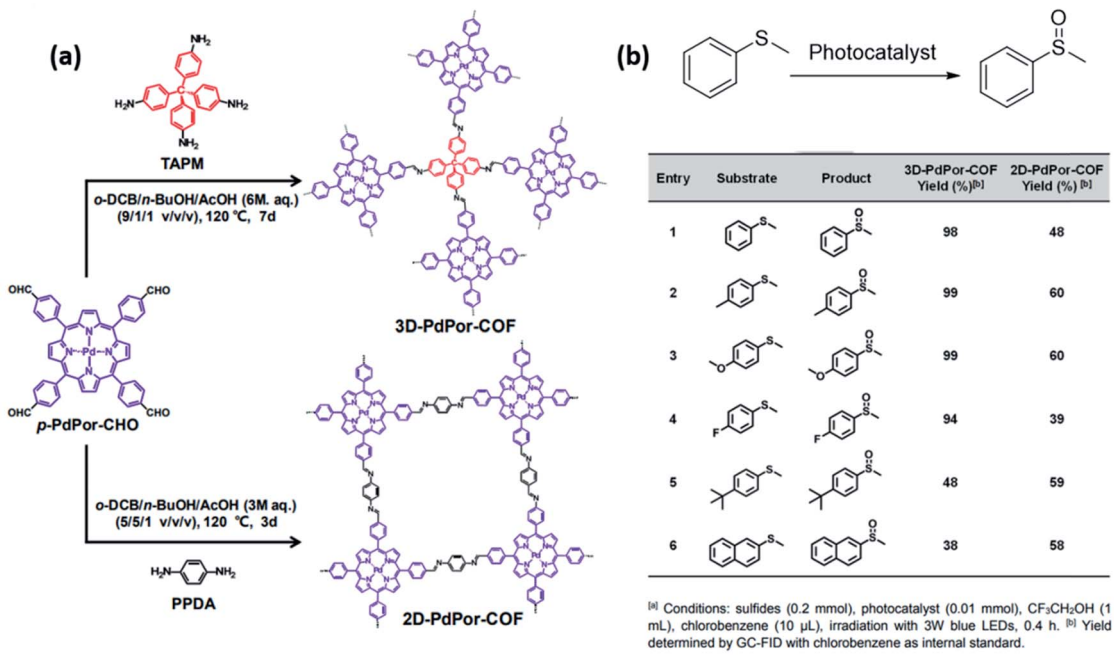

Entry	Substrate	Product	3D-PdPor-COF Yield (%)[b]	2D-PdPor-COF Yield (%)[b]
1			98	48
2			99	60
3			99	60
4			94	39
5			48	59
6			38	58

[a] Conditions: sulfides (0.2 mmol), photocatalyst (0.01 mmol), CF_3CH_2OH (1 mL), chlorobenzene (10 μL), irradiation with 3W blue LEDs, 0.4 h. [b] Yield determined by GC-FID with chlorobenzene as internal standard.

Fig. 18 (a) Schematic diagram of the synthesis of the porphyrinic COFs. (b) Substrate scope of the photocatalytic selective oxidation of sulfides to sulfoxides. Adapted from ref. 107 with the permission of John Wiley and Sons, Copyright 2019.

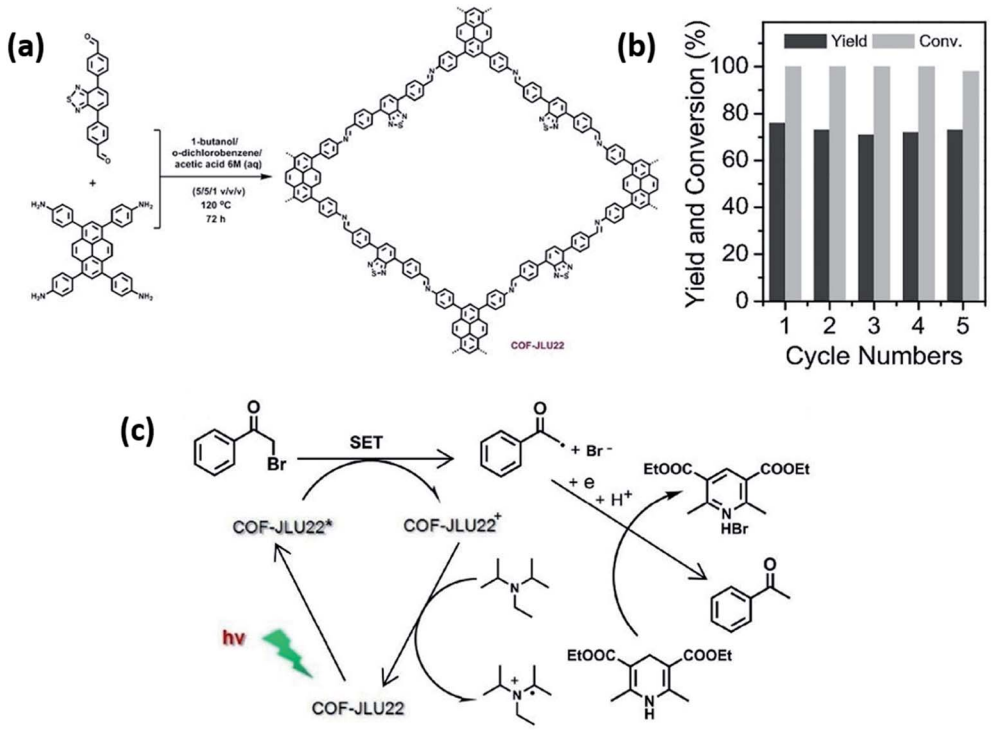

Fig. 19 (a) Schematic illustration of the synthesis of COF-JLU22. (b) Photostability test of the photoreductive dehalogenation of phenacyl bromide by COF-JLU22. (c) Proposed mechanism for the photoreductive reaction. Adapted from ref. 109 with the permission of Elsevier B.V., Copyright 2019.

(Pd) doped MOF@COF hybrid in the form of Pd/TiATA@LZU-1 was reported and tested for photocatalytic hydrogenation of various kinds of olefins, in which Pd nanoparticles were the active centers, the MOF core acted as the electron donor and the COF shell served as a mediator for electron transfer. Compared with the pristine TiATA, Pd/TiATA or TiATA@LZU-1, the Pd/TiATA@LZU-1 core–shell composite exhibited much better photocatalytic activity (99% conversion and selectivity of styrene in 15 min).[112]

Coupling reactions are another important branch of the field of organic synthesis. Liu and co-workers employed a newly designed D–A type imine-linked COF (COF-JLU5) as the photocatalyst for efficient aerobic cross-dehydrogenative coupling (CDC) reaction of *N*-aryltetrahydroisoquinolines (Fig. 20a). The high porosity, crystallinity, superior stability, and columnar π-arrays as well as excellent photoredox properties of COF-JLU5 endowed it with excellent photocatalytic activity and recyclability towards a variety of substrates with different substituted groups (Fig. 20b), and a possible reaction mechanism for the aerobic photocatalytic C–H functionalization under visible-light irradiation is shown in Fig. 20c. More interestingly, C–P bonds can also be formed with phosphonates as the nucleophilic reagents and COF-JLU5 as the photocatalyst.[113]

Recently, Wu *et al.* studied the same reaction by employing a hydrozone-linked TFB-COF as the photocatalyst and the experimental results revealed that the position and electron-deficient/rich properties of the substituent groups have great effects on the photocatalytic activity of the COF catalyst.[114]

Selective oxidative coupling of amines to imines is of fundamental importance for the synthesis of biologically and pharmaceutically active products.[115,116] Very recently, the Wu group reported a highly hydrophilic hydrazone-based TFPT-BMTH-COF by incorporating 2-methoxyethoxy groups into the channel walls of the COF material, which was further evaluated for photooxidative coupling of benzyl amine derivatives at room temperature under an air atmosphere. The experimental results indicated that the derivatives with electron-withdrawing groups generally showed low conversion due to the strong electron-deficient effect of the substituents by destabilizing cationic radical intermediates, which was the key species to proceed the photocatalytic reactions.[117]

The importance and practicality of asymmetric reactions as effective tools to obtain enantiomerically pure compounds has been fully acknowledged by scientists in the chemical, pharmaceutical, medicinal and agricultural industries.[118] Very recently, Cui and co-workers prepared two twofold interpenetrated 3D COFs with the ffc topology and for the first time explored their photocatalytic activity for asymmetric α-alkylation of aldehydes with a MacMillan imidazolidinone as the chiral catalyst. Impressively, the obtained COFs exhibited significantly high yields up to 94% enantiomeric excess, comparable to many molecular metal complexes and organic dyes as the photosensitizers. Interestingly, the COF photocatalysts lost their crystallinity after catalysis and they could be readily recrystallized *via* a solvent-assisted building unit exchange and reused with negligible loss of their photocatalytic

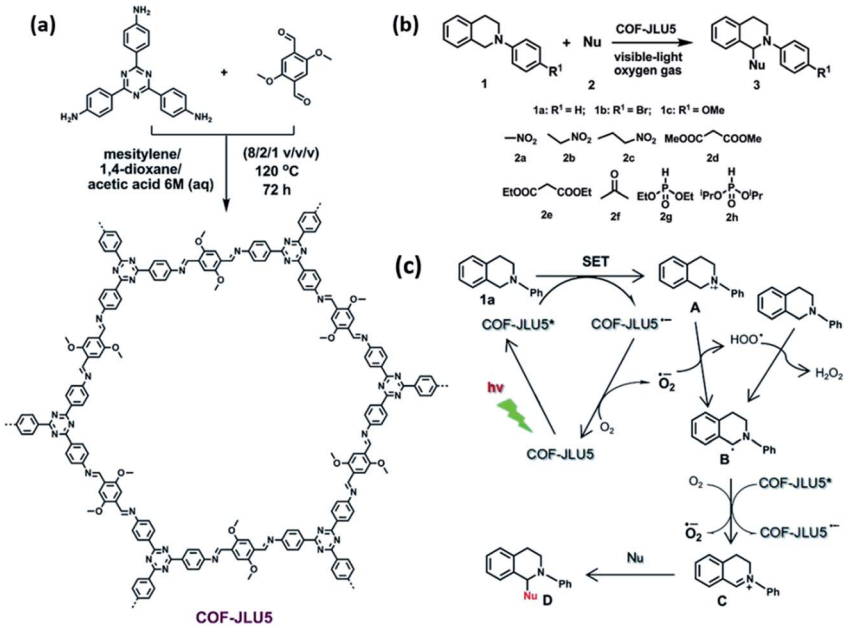

Fig. 20 (a) Schematic illustration of the synthesis of COF-JLU5. (b) Photocatalytic aerobic CDC of *N*-aryltetrahydroisoquinolines with a wide variety of nucleophiles. (c) Proposed mechanism for the aerobic photocatalytic C-H functionalization reaction. Reproduced with the permission of ref. 113. Copyright 2017, Royal Society of Chemistry.

activity. This study paved the way of COFs for future possible photoredox asymmetric catalysis.[119]

Besides the abovementioned crucial reactions in photoredox organic transformations, several other reactions, such as the arylation and alkylation of quinoxalin-2(1*H*)-ones with hydrazines,[120,121] polymerization of methyl methacrylate,[122] Alder–Ene reaction,[123] and *trans* (*E*) to *cis* (*Z*) isomerization of olefins,[124] have also been exploited employing COF-based materials as the photocatalysts.

3.4. COFs for degradation of organic contaminants

Organic dyes (*e.g.* methylene blue (MB), methyl orange (MO), rhodamine B (RhB) and Congo red (CR)) from the leather, paper and food industries and heavy metals (*e.g.* $Cr^{(VI)}$) with non-biodegradability from the leather, printing and pigment industries are the two major types of water pollutants that are highly toxic and pose serious threats to humans and to the environment. In recent years, photocatalytic degradation of these contaminants has been one of the intensely studied topics in the field of environmental science. The degradation process of the pollutants using semiconductors is relatively complicated and a general possible mechanism was provided by Liu and co-workers.[18] COFs, as a new burgeoning type of advanced crystalline porous material, have recently been explored as efficient photocatalysts for degradation of these pollutants. Cai *et al.* reported a set of imine-based COFs (COF_{A+B}, COF_{A+C} and COF_{A+D}) (Fig. 21a) that were further employed for the photodegradation of MO in water and the structure–property relationships were systematically investigated. After 30 min visible-light irradiation, COF_{A+C} can completely degrade MO, while only 29.6% MO was decomposed by COF_{A+B} and almost no degradation of MO dye was observed for COF_{A+D} (Fig. 21b–e), which was mainly attributed to the higher conjugation degree and higher density of the visible-light active centers (triazine ring) in the structure of COF_{A+C}.[125] Zhao and co-workers studied the photocatalytic degradation of phenol and MO performance on a TpMA COF, which was prepared by a ball milling mechanochemical method at ambient temperature for a shorter time instead of a solvothermal method at high temperature and longer reaction time. More importantly, the photocatalytic performance of the obtained COF is comparable with that of the COF synthesized under solvothermal conditions.[126]

As mentioned above, COFs can also serve as ideal supports to composite with other photoactive species to further improve their photocatalytic activities. Along these lines, Wang *et al.* reported the assembly of g-C_3N_4 and COFs through a simple thermal treatment to obtain hierarchical g-C_3N_4@COFs composites for the photocatalytic removal of orangeII. Remarkably, the hybrids exhibited an orangeII removal efficiency of 100% compared to the pristine g-C_3N_4 (10%) and COF (5%), which was mainly derived from the high surface area, nitrogen dopant and conductive carbon networks.[127] Tan and co-workers developed a new strategy to prepare a type of carbon nitride (PCN-1 and PCN-2) by introducing a heptazine unit into the backbone of a triazine-based COF and the obtained hybrids exhibited excellent photocatalytic performance towards RhB degradation.[128] Jiang *et al.* reported a set of CuPor-Ph-COF/g-C_3N_4 composites through *in situ* synthesis on the surface of g-C_3N_4 by a facile liquid-assisted grinding method and the as-prepared composite displayed superior photocatalytic activity of RhB degradation under visible-light irradiation compared to that of the pure g-C_3N_4 or CuPor-Ph-COF due to the faster

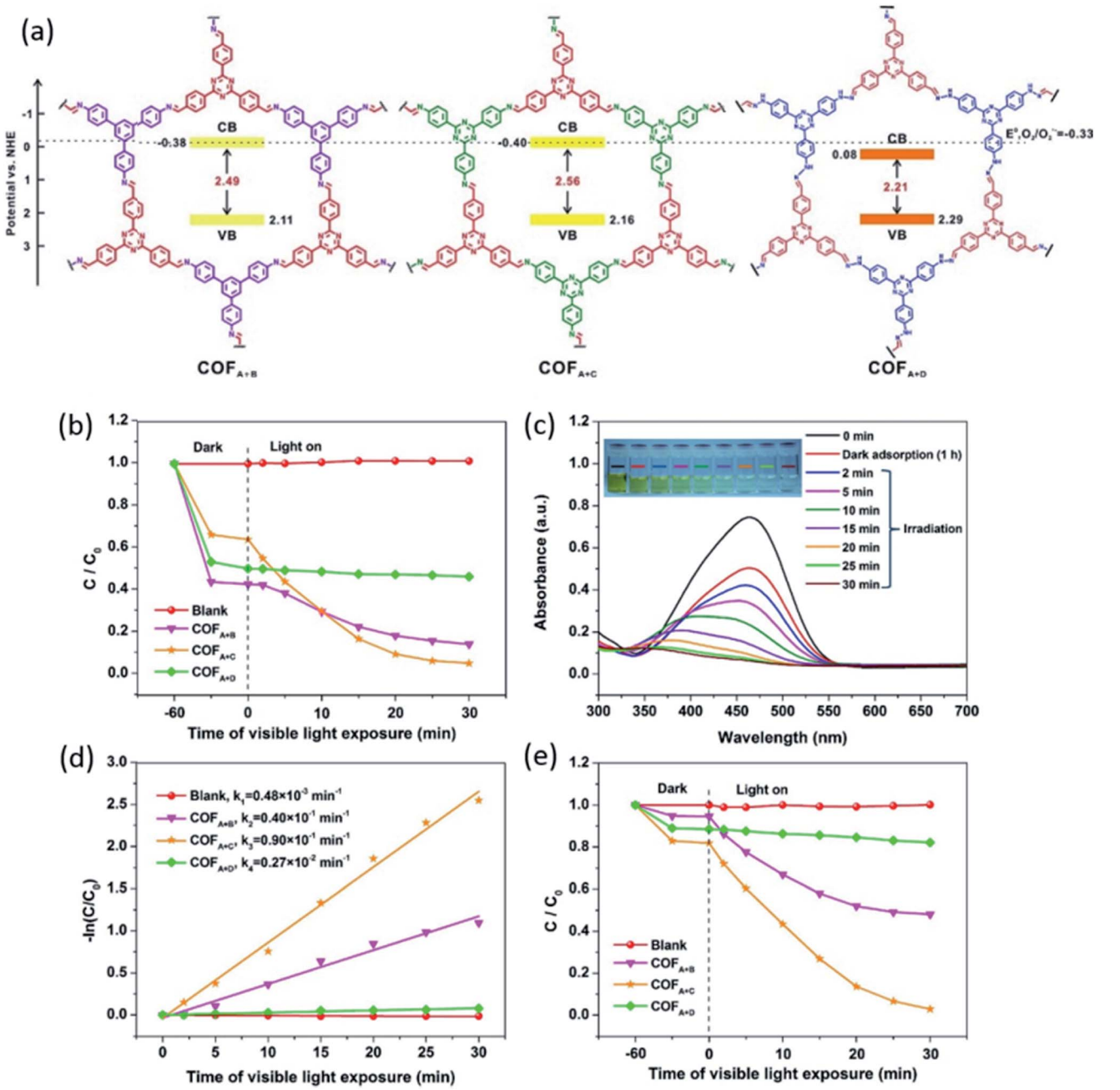

Fig. 21 (a) The structure and related band alignment of COF_{A+B}, COF_{A+C} and COF_{A+D}. (b to e) Photocatalytic results over the studied COFs under visible-light irradiation. Adapted from ref. 125 with permission from Elsevier B.V. Copyright 2019.

separation of photoexcited charges.[129] TiO_2 represents one of the most widely studied photocatalysts for a broad range of photocatalytic applications. The Zhang group reported a simple and mild synthetic approach to prepare ultrafine Fe-doped TiO_2 nanoparticles by using the crystalline TpTa-COF as the support. Remarkably, the resulting hybrid photocatalyst, 5Fe-TiO_2@-COF, showed unprecedented MB photocatalytic degradation efficiency in the absence of any external oxidant and the superior performance was claimed to be derived from the small size and large surface area of the nanoparticles, the narrower band gap due to Fe-doping, and the excellent MB adsorption by the COF support.[130] The assembly of MOFs and COFs to form the heterojunction for modulating their optical, electronic and redox properties has been proven to be an effective approach to achieve better photocatalytic performance.[57,112] Very recently, Zhang and co-workers reported a new type of MOF@COF core–shell hybrid material by integration of NH_2-MIL-68 and TPA-COF for the degradation of RhB under visible-light irradiation ($\lambda > 420$ nm) for the first time and the obtained hybrid material exhibited better photocatalytic activity with a rate constant of 0.077 min^{-1}, which was about 1.4 times that of the pure NH_2-MIL-68 material due to the enhanced surface area (539 m^2g^{-1}

vs. 451 m^2g^{-1}) and reduced band gaps (2.21 eV *vs.* 2.82 eV).[131] Similarly, Wang and co-workers synthesized two novel photoactive MOF@COF-based materials, *i.e.* MIL-101-NH_2@TpMA-COF and UiO-66-NH_2@TpMA-COF, for photocatalytic degradation of bisphenol (BPA). The experimental results revealed that the MOF@COF hybrid materials can effectively improve the photocatalytic activities compared with those of the pure MOF or COF materials due to the fact that the heterojunction formed at the interface can effectively facilitate the transport and separation of the photoexcited electron–hole pairs.[132] A similar study was recently reported by Cai and co-workers, who reported a series of covalently integrated MOF/COF hybrid materials by encapsulating different MOFs (NH_2-MIL-125(Ti), NH_2-UiO-66 and NH_2-MIL-53) with highly stable TTB-TTA-COF (TTB = 4,4′,4″-(1,3,5-triazine2,4,6-triyl)tribenzaldehyde and TTA = 4,4′,4″-(1,3,5-triazine-2,4,6-triyl)trianiline) (Fig. 22). The formation of the heterojunction can tune their optical properties and promote charge separation, thus resulting in enhanced photocatalytic activities as confirmed by the photocatalytic degradation of phenol and MO. For example, the NH_2-MIL-125(Ti)/TTB-TTA-COF composite exhibited a much higher photodegradation kinetics of MO, which was 9 and 2 times the rates of pure NH_2-MIL-125(Ti) and TTB-TTA-COF.[133]

In a subclass of COFs termed as nitrogen-rich porous organic polymers, recent studies have revealed the great potential of CTFs as photoactive catalysts for diverse photocatalytic applications due to their extraordinary chemical stability as well as their semiconductor characters with broad light absorption in the visible light range.[10,134] In 2014, Song and co-workers employed CTF-1 as the photocatalyst for the degradation of the organic dye MB under visible-light irradiation, which exhibited almost total degradation efficiency in 1 h and the photocatalyst can be reused for several cycles without a significant decrease in the photocatalytic activity.[135] Zhang *et al.* reported a novel BiOBr/CTF-3D nanocomposite photocatalyst *via* a simple co-precipitation approach for the degradation of antibiotics (*e.g.* tetracycline hydrochloride and ciprofloxacin) under visible-light irradiation. The trapping experiments of the active species confirmed that $^{\bullet}O_2^-$ was the main radical species for photocatalysis, and the synergistic effects of the enlarged optical adsorption range, the efficient photogenerated electron–hole pair separation and the accelerated adsorption and transfer of antibiotic molecules resulted in increased photocatalytic activity after the doping of CTF-3D.[136]

Hexavalent chromium ($Cr^{(VI)}$), as a ubiquitous heavy metal ion, has become one of the major environmental pollutants metabolized in industrial production, which not only is a lasting hazard to the environment, but also possibly causes cancer in humans. Photocatalysis, as a means to convert $Cr^{(VI)}$ to relatively low-toxic $Cr^{(III)}$ by the use of sustainable solar energy and suitable photocatalysts, has attracted widespread attention in recent years. However, the use of COFs as the photocatalyst for reduction of $Cr^{(VI)}$ is still rare. Chen and co-workers reported two D-A based COFs by using tris(4-aminophenyl)benzene (TPB) and tris-(4-aminophenyl)triazine (TAPT) as the donor units and benzo[*c*][1,2,5]thiadiazole-4,7-dicarbaldehyde (BT) as the acceptor building block, which were further applied for the photocatalytic reduction of aqueous $Cr^{(VI)}$ (Fig. 23a). Remarkably, over 99% $Cr^{(VI)}$ was reduced to $Cr^{(III)}$ by utilizing TPB-BT-COF as the photocatalyst without any sacrificial agents or additional pH regulation. The photocatalysis rate of TPB-BT-COF was higher than that of TAPT-BT-COF, which was mainly due to the more negative conduction band, narrower band gap and better photogenerated electron/

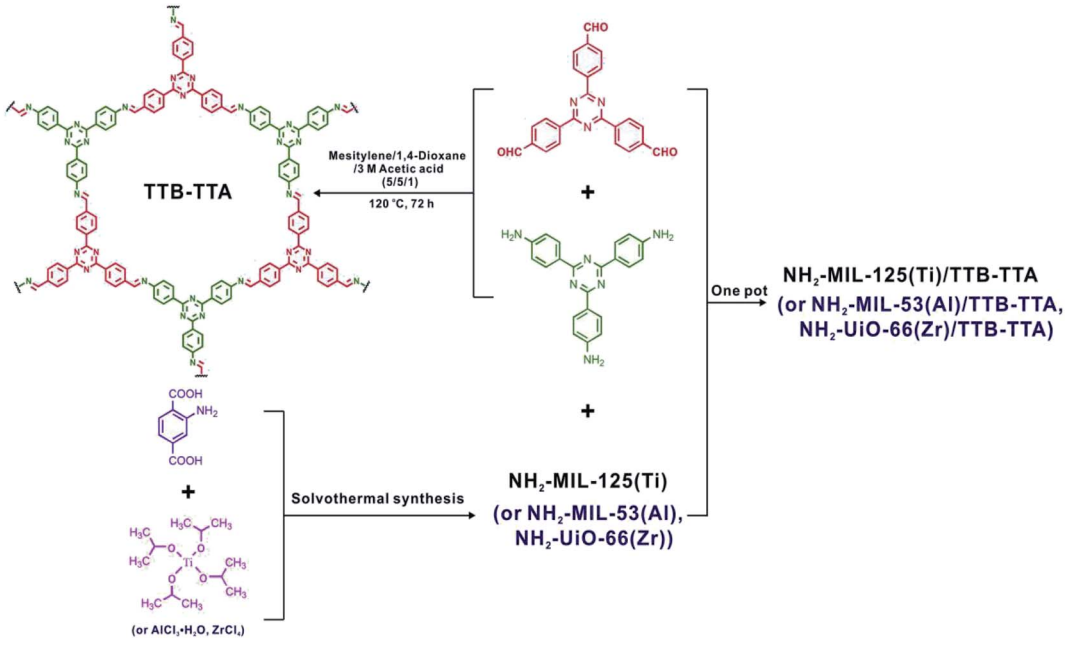

Fig. 22 Schematic representation of the preparation of the MOF/COF hybrid materials. Reproduced from ref. 133 with permission from Elsevier B.V. Copyright 2019.

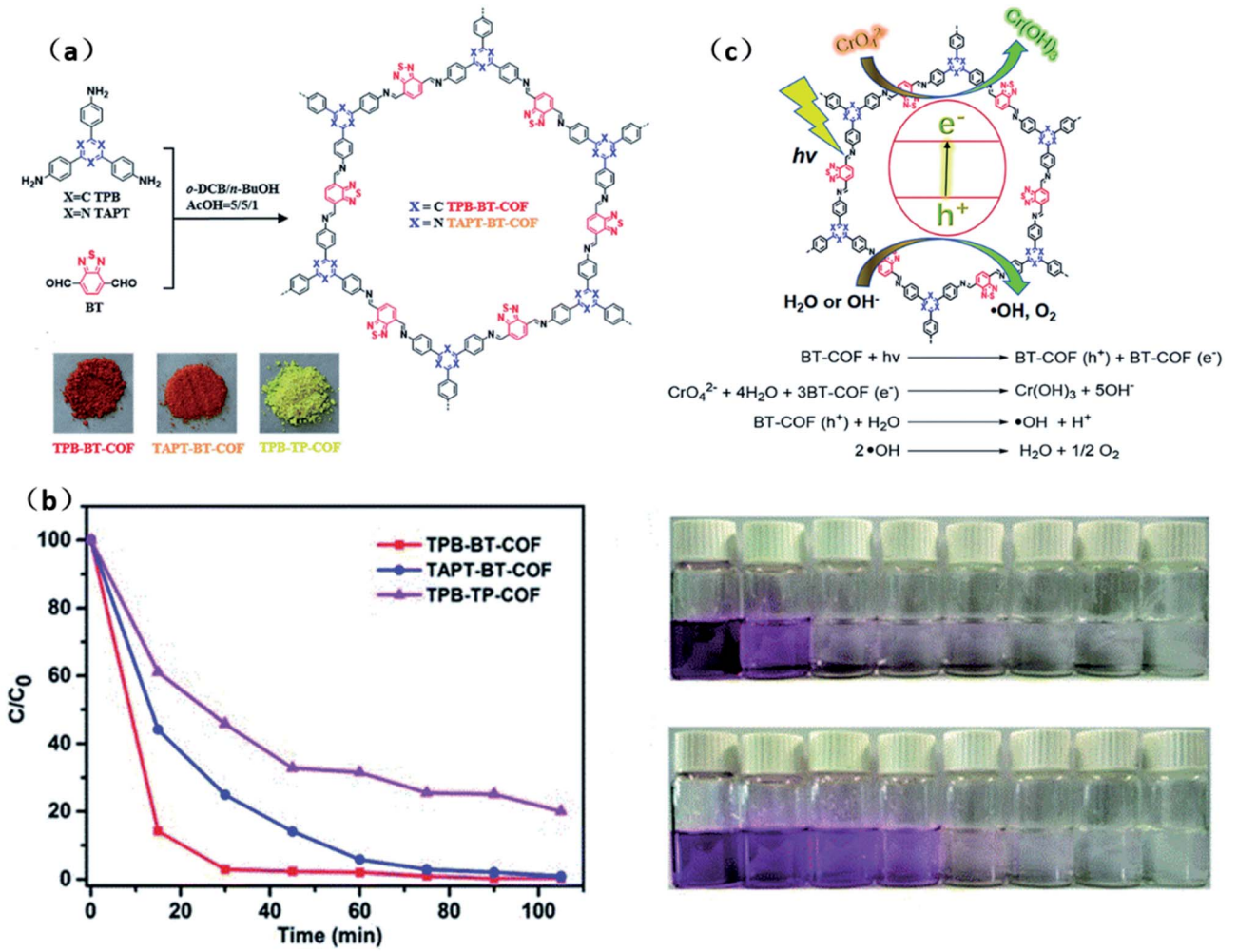

Fig. 23 (a) Schematic illustration of the BT-COF synthesis. (b) The photocatalytic rate comparison and the corresponding photographs of TPB-BT-COF and TAPT-BT-COF. (c) The proposed mechanism of photo-reduction of $Cr^{(VI)}$ by the BT-COFs. Reproduced from ref. 137 with permission from the Royal Society of Chemistry, Copyright 2019.

hole pair separation and migration of TPB-BT-COF (Fig. 23b and c).[137] Pi *et al.* reported a variety of novel La^{3+}- and Sb^{3+}- doped MOF-In_2S_3@FcDc-TAPT COFs for photocatalytic $Cr^{(VI)}$ reduction under visible-light irradiation. The experimental results demonstrated that doping lanthanide ions can significantly improve the photocatalytic efficiency of $Cr^{(VI)}$ of the composites. In particular, Sb^{3+}-doped MOF-In_2S_3@FcDc-TAPT COFs exhibited a $Cr^{(VI)}$ removal efficiency of 99% within 20 min and the kinetics constant for $Cr^{(VI)}$ reduction was 0.437 min^{-1}, which was 20-fold higher than that of the non-doped hybrid material and the removal efficiency even had no significant changes after 150 days.[138]

4. Conclusions and perspectives

Covalent organic frameworks represent a fascinating type of highly crystalline porous material that allows the atomically precise integration of specific building units into extended periodic structures with intriguing structural tunability and diversity. In particular, the semiconducting properties of COFs have empowered them as one of the most promising photocatalysts for diverse photocatalytic applications in recent years. In this review, we have provided a comprehensive and up-to-date overview of the development of COFs and their applications that have been realized so far, including photocatalytic hydrogen evolution, photocatalytic CO_2 reduction, photoredox reactions and photocatalytic degradation of organic pollutants. In spite of the substantial progress and achievements that have been made in recent years, the investigation of COFs for photocatalytic applications is still in its infancy and there are some crucial issues and challenges that still deserve further consideration to improve the photocatalytic efficiency of COF-based materials for photocatalysis applications.

(1) The developments of photocatalytic hydrogen evolution using COFs have evolved rapidly in the past few years and a benchmark hydrogen evolution rate of 23.41 mmol g^{-1} h^{-1} has been achieved, which is quite competitive to that of lots of inorganic semiconductors. However, most of the reported COFs still suffer from relatively low photocatalytic activity and to overcome this issue, the combination of D–A, D–A–A or D–A–D

moieties in the framework of COFs is anticipated to be a promising approach to enhance their photocatalytic performance due to the beneficial properties of the D–A structure for charge generation, mobility and stability. Another effective strategy is the proper combination of one or more species with COFs to form a heterojunction or composites that can facilitate the charge separation efficiency and improve the stability of the photocatalysts, thus resulting in improved photocatalytic activity. Another challenge in the field of photocatalytic hydrogen evolution is the exploration of alternatives to the noble platinum co-catalyst, and installing earth-abundant and low-cost metal-based catalytic centers into COFs has been proven to be an efficient approach. Apart from photocatalytic water reduction, photocatalytic water oxidation to produce O_2 using COFs as the photocatalysts is still infant, as water oxidation proceeds with greater difficulty in kinetic and energetic aspects; it is highly expected that more attention will be given and efforts made in the future to design more efficient COFs and exploit their potential for this application.

(2) The solar-driven reduction of CO_2 to valuable chemical fuels is a promising avenue to address the energy shortage and environment related problems; however, quite a few COFs have been exploited for this application until now and their photocatalytic performance was quite limited compared with that of state-of-the-art photocatalysts. The construction of a Z-scheme or heterostructures by coupling different semiconductors with properly aligned band structures is an effective way to enhance their photocatalytic properties. In particular, heterogeneous photoelectrochemical reduction of CO_2 on COFs should be considered as a possible approach to achieve efficient CO_2 utilization in the future. Furthermore, the combination of experimental and computational calculations to reveal the mechanism and real pathway of the reaction is of fundamental importance to guide researchers in multidisciplinary areas to design and develop more efficient photocatalysts for photocatalytic CO_2 reduction.

(3) The study and development of COF-based photocatalysts has rapidly expanded the toolbox of organic transformations and these photocatalysts displayed superior photocatalytic activity and recyclability for diverse photoredox reactions. However, compared with the traditional transition-metal complexes, the developed reaction types and substrate scope are still quite limited. Thus, it is highly desirable to exploit some challenging and crucial organic reactions, such as asymmetric reactions and C–C functionalization reactions. Another important issue for the development of photoactive COFs is their long-term stability under harsh conditions. The recently reported sp^2 carbon and dioxin linkage based COFs have exhibited exceptionally high chemical stability even in concentrated acid and base solutions, which should be beneficial for their possible practical applications in the future.

(4) As for the application of photodegradation of organic contaminants, the wettability or good water dispersion of COFs and their high stability are significantly important to achieve better photocatalytic activity. Thus, the incorporation of some desired functional groups into the structure of COFs to construct stable hydrophilic COFs is highly expected. A detailed study of their photocatalytic performance under real life conditions would be more valuable to promote and accelerate their practical applications.

Despite their relatively short history of development, the pioneering and prominent studies have unambiguously demonstrated the great potential of COFs for diverse photocatalysis applications and there is no doubt that the development of COF-based photocatalyst materials will open up new avenues for efficient utilization of solar energy for energy- and environment-related applications.

Conflicts of interest

The authors declare no conflicts of interest.

Acknowledgements

We are grateful for financial support from the National Natural Science Foundation of China (Grant No. 21671122, 21772116 and 21971153), the Taishan Scholar's Construction Project of Shandong Province, and Chang Jiang Scholars Program of China at SDNU.

References

1 A. Kudo and Y. Miseki, *Chem. Soc. Rev.*, 2009, **38**, 253–278.
2 W. Tu, Y. Zhou and Z. Zou, *Adv. Mater.*, 2014, **26**, 4607–4626.
3 C. Wang, Z. Sun, Y. Zheng and Y. H. Hu, *J. Mater. Chem. A*, 2019, **7**, 865–887.
4 J. Xuan and W.-J. Xiao, *Angew. Chem., Int. Ed.*, 2012, **51**, 6828–6838.
5 W. Doerffler and K. Hauffe, *J. Catal.*, 1964, **3**, 171–178.
6 F. Steinbach, *Nature*, 1969, **221**, 657–658.
7 A. Fujishima and K. Honda, *Nature*, 1972, **238**, 37–38.
8 J. H. Carey, J. Lawrence and H. M. Tosine, *Bull. Environ. Contam. Toxicol.*, 1976, **16**, 697–701.
9 T. Inoue, A. Fujishima, S. Konishi and K. Honda, *Nature*, 1979, **277**, 637–638.
10 T. Zhang, G. Xing, W. Chen and L. Chen, *Mater. Chem. Front.*, 2020, **4**, 332–353.
11 Y. Wang, A. Vogel, M. Sachs, R. S. Sprick, L. Wilbraham, S. J. A. Moniz, R. Godin, M. A. Zwijnenburg, J. R. Durrant, A. I. Cooper and J. Tang, *Nat. Energy*, 2019, **4**, 746–760.
12 A. P. Côté, A. I. Benin, N. W. Ockwig, M. Keeffe, A. J. Matzger and O. M. Yaghi, *Science*, 2005, **310**, 1166.
13 Y. Zeng, R. Zou and Y. Zhao, *Adv. Mater.*, 2016, **28**, 2855–2873.
14 S.-Y. Ding and W. Wang, *Chem. Soc. Rev.*, 2013, **42**, 548–568.
15 Q. Guan, L. L. Zhou, Y. A. Li, W. Y. Li, S. Wang, C. Song and Y. B. Dong, *ACS Nano*, 2019, **13**, 13304–13316.
16 Q. Guan, D.-D. Fu, Y.-A. Li, X.-M. Kong, Z.-Y. Wei, W.-Y. Li, S.-J. Zhang and Y.-B. Dong, *iScience*, 2019, **14**, 180–198.
17 X. Liu, D. Huang, C. Lai, G. Zeng, L. Qin, H. Wang, H. Yi, B. Li, S. Liu, M. Zhang, R. Deng, Y. Fu, L. Li, W. Xue and S. Chen, *Chem. Soc. Rev.*, 2019, **48**, 5266–5302.
18 C. Dai and B. Liu, *Energy Environ. Sci.*, 2020, **13**, 24–52.

19 S. Wan, J. Guo, J. Kim, H. Ihee and D. Jiang, *Angew. Chem., Int. Ed.*, 2008, **47**, 8826–8830.
20 D. Jiang, X. Chen, K. Geng, R. Liu, K. T. Tan, Y. Gong, Z. Li, S. Tao and Q. Jiang, *Angew. Chem., Int. Ed.*, 2019, DOI: 10.1002/anie.201904291.
21 M. S. Lohse and T. Bein, *Adv. Funct. Mater.*, 2018, **28**, 1705553.
22 G. N. Lewis, *J. Am. Chem. Soc.*, 1916, **38**, 762–785.
23 R. Hoffmann, *Sci. Am.*, 1993, **268**, 66–73.
24 H. M. El-Kaderi, J. R. Hunt, J. L. Mendoza-Cortés, A. P. Côté, R. E. Taylor, M. Keeffe and O. M. Yaghi, *Science*, 2007, **316**, 268.
25 F. J. Uribe-Romo, J. R. Hunt, H. Furukawa, C. Klöck, M. O'Keeffe and O. M. Yaghi, *J. Am. Chem. Soc.*, 2009, **131**, 4570–4571.
26 G. Wang, N. Tahir, I. Onyshchenko, N. De Geyter, R. Morent, K. Leus and P. Van Der Voort, *Microporous Mesoporous Mater.*, 2019, **290**, 109650.
27 G. Wang, Y. Onyshchenko, N. De Geyter, R. Morent, K. Leus and P. Van Der Voort, *Dalton Trans.*, 2019, **48**, 17612–17619.
28 G. Wang, K. Leus, H. S. Jena, C. Krishnaraj, S. Zhao, H. Depauw, N. Tahir, Y.-Y. Liu and P. Van Der Voort, *J. Mater. Chem. A*, 2018, **6**, 6370–6375.
29 M. Liu, L. Guo, S. Jin and B. Tan, *J. Mater. Chem. A*, 2019, **7**, 5153–5172.
30 P. Kuhn, M. Antonietti and A. Thomas, *Angew. Chem., Int. Ed.*, 2008, **47**, 3450–3453.
31 S. Ren, M. J. Bojdys, R. Dawson, A. Laybourn, Y. Z. Khimyak, D. J. Adams and A. I. Cooper, *Adv. Mater.*, 2012, **24**, 2357–2361.
32 K. Wang, L.-M. Yang, X. Wang, L. Guo, G. Cheng, C. Zhang, S. Jin, B. Tan and A. Cooper, *Angew. Chem., Int. Ed.*, 2017, **56**, 14149–14153.
33 T. Ma, E. A. Kapustin, S. X. Yin, L. Liang, Z. Zhou, J. Niu, L.-H. Li, Y. Wang, J. Su, J. Li, X. Wang, W. D. Wang, W. Wang, J. Sun and O. M. Yaghi, *Science*, 2018, **361**, 48.
34 A. M. Evans, L. R. Parent, N. C. Flanders, R. P. Bisbey, E. Vitaku, M. S. Kirschner, R. D. Schaller, L. X. Chen, N. C. Gianneschi and W. R. Dichtel, *Science*, 2018, **361**, 52.
35 L. Stegbauer, K. Schwinghammer and B. V. Lotsch, *Chem. Sci.*, 2014, **5**, 2789–2793.
36 F. J. Uribe-Romo, C. J. Doonan, H. Furukawa, K. Oisaki and O. M. Yaghi, *J. Am. Chem. Soc.*, 2011, **133**, 11478–11481.
37 S. Dalapati, S. Jin, J. Gao, Y. Xu, A. Nagai and D. Jiang, *J. Am. Chem. Soc.*, 2013, **135**, 17310–17313.
38 Q. Fang, Z. Zhuang, S. Gu, R. B. Kaspar, J. Zheng, J. Wang, S. Qiu and Y. Yan, *Nat. Commun.*, 2014, **5**, 4503.
39 E. Jin, M. Asada, Q. Xu, S. Dalapati, M. A. Addicoat, M. A. Brady, H. Xu, T. Nakamura, T. Heine, Q. Chen and D. Jiang, *Science*, 2017, **357**, 673.
40 H. Lyu, C. S. Diercks, C. Zhu and O. M. Yaghi, *J. Am. Chem. Soc.*, 2019, **141**, 6848–6852.
41 H. Wu, H. L. Tan, C. Y. Toe, J. Scott, L. Wang, R. Amal and Y. H. Ng, *Adv. Mater.*, 2019, 1904717.
42 V. S. Vyas, F. Haase, L. Stegbauer, G. Savasci, F. Podjaski, C. Ochsenfeld and B. V. Lotsch, *Nat. Commun.*, 2015, **6**, 8508.
43 L. Stegbauer, S. Zech, G. Savasci, T. Banerjee, F. Podjaski, K. Schwinghammer, C. Ochsenfeld and B. V. Lotsch, *Adv. Energy Mater.*, 2018, **8**, 1703278.
44 J.-L. Sheng, H. Dong, X.-B. Meng, H.-L. Tang, Y.-H. Yao, D.-Q. Liu, L.-L. Bai, F.-M. Zhang, J.-Z. Wei and X.-J. Sun, *ChemCatChem*, 2019, **11**, 2313–2319.
45 P. Pachfule, A. Acharjya, J. Roeser, T. Langenhahn, M. Schwarze, R. Schomäcker, A. Thomas and J. Schmidt, *J. Am. Chem. Soc.*, 2018, **140**, 1423–1427.
46 L. Y. Li, Z. M. Zhou, L. Y. Li, Z. Y. Zhuang, J. H. Bi, J. H. Chen, Y. Yu and J. G. Yu, *ACS Sustainable Chem. Eng.*, 2019, **7**, 18574–18581.
47 R. S. Sprick, Y. Bai, A. A. Y. Guilbert, M. Zbiri, C. M. Aitchison, L. Wilbraham, Y. Yan, D. J. Woods, M. A. Zwijnenburg and A. I. Cooper, *Chem. Mater.*, 2019, **31**, 305–313.
48 Y. B. Zhao, W. Y. Ma, Y. F. Xu, C. Zhang, Q. Wang, T. J. Yang, X. M. Gao, F. Wang, C. Yan and J. X. Jiang, *Macromolecules*, 2018, **51**, 9502–9508.
49 X. Wang, L. Chen, S. Y. Chong, M. A. Little, Y. Wu, W.-H. Zhu, R. Clowes, Y. Yan, M. A. Zwijnenburg, R. S. Sprick and A. I. Cooper, *Nat. Chem.*, 2018, **10**, 1180–1189.
50 T. Banerjee and B. V. Lotsch, *Nat. Chem.*, 2018, **10**, 1175–1177.
51 J. Thote, H. B. Aiyappa, A. Deshpande, D. DíazDíaz, S. Kurungot and R. Banerjee, *Chem.–Eur. J.*, 2014, **20**, 15961–15965.
52 M.-Y. Gao, C.-C. Li, H.-L. Tang, X.-J. Sun, H. Dong and F.-M. Zhang, *J. Mater. Chem. A*, 2019, **7**, 20193–20200.
53 Y.-J. Cheng, R. Wang, S. Wang, X.-J. Xi, L.-F. Ma and S.-Q. Zang, *Chem. Commun.*, 2018, **54**, 13563–13566.
54 J. Wen, J. Xie, X. Chen and X. Li, *Appl. Surf. Sci.*, 2017, **391**, 72–123.
55 W.-J. Ong, L.-L. Tan, Y. H. Ng, S.-T. Yong and S.-P. Chai, *Chem. Rev.*, 2016, **116**, 7159–7329.
56 M. Luo, Q. Yang, K. Liu, H. Cao and H. Yan, *Chem. Commun.*, 2019, **55**, 5829–5832.
57 F.-M. Zhang, J.-L. Sheng, Z.-D. Yang, X.-J. Sun, H.-L. Tang, M. Lu, H. Dong, F.-C. Shen, J. Liu and Y.-Q. Lan, *Angew. Chem., Int. Ed.*, 2018, **57**, 12106–12110.
58 E. Jin, Z. Lan, Q. Jiang, K. Geng, G. Li, X. Wang and D. Jiang, *Chem*, 2019, **5**, 1632–1647.
59 S. Wei, F. Zhang, W. Zhang, P. Qiang, K. Yu, X. Fu, D. Wu, S. Bi and F. Zhang, *J. Am. Chem. Soc.*, 2019, **141**, 14272–14279.
60 S. Bi, C. Yang, W. Zhang, J. Xu, L. Liu, D. Wu, X. Wang, Y. Han, Q. Liang and F. Zhang, *Nat. Commun.*, 2019, **10**, 2467.
61 T. Banerjee, F. Haase, G. Savasci, K. Gottschling, C. Ochsenfeld and B. V. Lotsch, *J. Am. Chem. Soc.*, 2017, **139**, 16228–16234.
62 B. P. Biswal, H. A. Vignolo-González, T. Banerjee, L. Grunenberg, G. Savasci, K. Gottschling, J. Nuss, C. Ochsenfeld and B. V. Lotsch, *J. Am. Chem. Soc.*, 2019, **141**, 11082–11092.

63 H. Dong, X.-B. Meng, X. Zhang, H.-L. Tang, J.-W. Liu, J.-H. Wang, J.-Z. Wei, F.-M. Zhang, L.-L. Bai and X.-J. Sun, *Chem. Eng. J.*, 2020, **379**, 122342.
64 J. Wang, J. Zhang, S. B. Peh, G. Liu, T. Kundu, J. Dong, Y. Ying, Y. Qian and D. Zhao, *Sci. China: Chem.*, 2019, **63**, 192–197.
65 J. Bi, W. Fang, L. Li, J. Wang, S. Liang, Y. He, M. Liu and L. Wu, *Macromol. Rapid Commun.*, 2015, **36**, 1799–1805.
66 L. Li, W. Fang, P. Zhang, J. Bi, Y. He, J. Wang and W. Su, *J. Mater. Chem. A*, 2016, **4**, 12402–12406.
67 Z. Cheng, W. Fang, T. Zhao, S. Fang, J. Bi, S. Liang, L. Li, Y. Yu and L. Wu, *ACS Appl. Mater. Interfaces*, 2018, **10**, 41415–41421.
68 L. Guo, Y. Niu, S. Razzaque, B. Tan and S. Jin, *ACS Catal.*, 2019, **9**, 9438–9445.
69 G. Zhou, L.-L. Zheng, D. Wang, Q.-J. Xing, F. Li, P. Ye, X. Xiao, Y. Li and J.-P. Zou, *Chem. Commun.*, 2019, **55**, 4150–4153.
70 L. Guo, Y. Niu, H. Xu, Q. Li, S. Razzaque, Q. Huang, S. Jin and B. Tan, *J. Mater. Chem. A*, 2018, **6**, 19775–19781.
71 W. Huang, Q. He, Y. Hu and Y. Li, *Angew. Chem., Int. Ed.*, 2019, **58**, 8676–8680.
72 N. Wang, G. Cheng, L. Guo, B. Tan and S. Jin, *Adv. Funct. Mater.*, 2019, 1904781.
73 J. Ming, A. Liu, J. Zhao, P. Zhang, H. Huang, H. Lin, Z. Xu, X. Zhang, X. Wang, J. Hofkens, M. B. J. Roeffaers and J. Long, *Angew. Chem., Int. Ed.*, 2019, **58**, 18290–18294.
74 F. Haase, T. Banerjee, G. Savasci, C. Ochsenfeld and B. V. Lotsch, *Faraday Discuss.*, 2017, **201**, 247–264.
75 Z.-A. Lan, Y. Fang, X. Chen and X. Wang, *Chem. Commun.*, 2019, **55**, 7756–7759.
76 S. Bi, Z.-A. Lan, S. Paasch, W. Zhang, Y. He, C. Zhang, F. Liu, D. Wu, X. Zhuang, E. Brunner, X. Wang and F. Zhang, *Adv. Funct. Mater.*, 2017, **27**, 1703146.
77 F. Li, D. Wang, Q.-J. Xing, G. Zhou, S.-S. Liu, Y. Li, L.-L. Zheng, P. Ye and J.-P. Zou, *Appl. Catal., B*, 2019, **243**, 621–628.
78 C. B. Meier, R. Clowes, E. Berardo, K. E. Jelfs, M. A. Zwijnenburg, R. S. Sprick and A. I. Cooper, *Chem. Mater.*, 2019, **31**, 8830–8838.
79 S. Kuecken, A. Acharjya, L. Zhi, M. Schwarze, R. Schomäcker and A. Thomas, *Chem. Commun.*, 2017, **53**, 5854–5857.
80 S.-Y. Ding, P.-L. Wang, G.-L. Yin, X. Zhang and G. Lu, *Int. J. Hydrogen Energ.*, 2019, **44**, 11872–11876.
81 D. Wang, H. Zeng, X. Xiong, M.-F. Wu, M. Xia, M. Xie, J.-P. Zou and S.-L. Luo, *Sci. Bull.*, 2019, **65**, 113–122.
82 D. Wang, X. Li, L.-L. Zheng, L.-M. Qin, S. Li, P. Ye, Y. Li and J.-P. Zou, *Nanoscale*, 2018, **10**, 19509–19516.
83 S. C. Roy, O. K. Varghese, M. Paulose and C. A. Grimes, *ACS Nano*, 2010, **4**, 1259–1278.
84 N.-N. Vu, S. Kaliaguine and T.-O. Do, *Adv. Funct. Mater.*, 2019, **29**, 1901825.
85 T. Zhang and W. Lin, *Chem. Soc. Rev.*, 2014, **43**, 5982–5993.
86 Y. Zhao, G. I. N. Waterhouse, G. Chen, X. Xiong, L.-Z. Wu, C.-H. Tung and T. Zhang, *Chem. Soc. Rev.*, 2019, **48**, 1972–2010.
87 R. K. Yadav, A. Kumar, N.-J. Park, K.-J. Kong and J.-O. Baeg, *J. Mater. Chem. A*, 2016, **4**, 9413–9418.
88 Y. Fu, X. Zhu, L. Huang, X. Zhang, F. Zhang and W. Zhu, *Appl. Catal., B*, 2018, **239**, 46–51.
89 J. L. White, M. F. Baruch, J. E. Pander, Y. Hu, I. C. Fortmeyer, J. E. Park, T. Zhang, K. Liao, J. Gu, Y. Yan, T. W. Shaw, E. Abelev and A. B. Bocarsly, *Chem. Rev.*, 2015, **115**, 12888–12935.
90 H. Takeda, K. Koike, H. Inoue and O. Ishitani, *J. Am. Chem. Soc.*, 2008, **130**, 2023–2031.
91 H. Zhang, J. Wei, J. Dong, G. Liu, L. Shi, P. An, G. Zhao, J. Kong, X. Wang, X. Meng, J. Zhang and J. Ye, *Angew. Chem., Int. Ed.*, 2016, **55**, 14310–14314.
92 R. Xu, X.-S. Wang, H. Zhao, H. Lin, Y.-B. Huang and R. Cao, *Catal. Sci. Technol.*, 2018, **8**, 2224–2230.
93 S. Yang, W. Hu, X. Zhang, P. He, B. Pattengale, C. Liu, M. Cendejas, I. Hermans, X. Zhang, J. Zhang and J. Huang, *J. Am. Chem. Soc.*, 2018, **140**, 14614–14618.
94 Z. Fu, X. Wang, A. M. Gardner, X. Wang, S. Y. Chong, G. Neri, A. J. Cowan, L. Liu, X. Li, A. Vogel, R. Clowes, M. Bilton, L. Chen, R. S. Sprick and A. I. Cooper, *Chem. Sci.*, 2020, **11**, 543–550.
95 S.-Y. Li, S. Meng, X. Zou, M. El-Roz, I. Telegeev, O. Thili, T. X. Liu and G. Zhu, *Microporous Mesoporous Mater.*, 2019, **285**, 195–201.
96 W. Liu, X. Li, C. Wang, H. Pan, W. Liu, K. Wang, Q. Zeng, R. Wang and J. Jiang, *J. Am. Chem. Soc.*, 2019, **141**, 17431–17440.
97 F. Wang, *ChemSusChem*, 2017, **10**, 4393–4402.
98 W. Zhong, R. Sa, L. Li, Y. He, L. Li, J. Bi, Z. Zhuang, Y. Yu and Z. Zou, *J. Am. Chem. Soc.*, 2019, **141**, 7615–7621.
99 J. Bi, B. Xu, L. Sun, H. Huang, S. Fang, L. Li and L. Wu, *ChemPlusChem*, 2019, **84**, 1149–1154.
100 M. Lu, Q. Li, J. Liu, F.-M. Zhang, L. Zhang, J.-L. Wang, Z.-H. Kang and Y.-Q. Lan, *Appl. Catal., B*, 2019, **254**, 624–633.
101 M. Lu, J. Liu, Q. Li, M. Zhang, M. Liu, J. L. Wang, D. Q. Yuan and Y. Q. Lan, *Angew. Chem., Int. Ed.*, 2019, **58**, 12392–12397.
102 G. Lu, X. Huang, Y. Li, G. Zhao, G. Pang and G. Wang, *J. Energy Chem.*, 2020, **43**, 8–15.
103 G. Lu, X. Huang, Z. Wu, Y. Li, L. Xing, H. Gao, W. Dong and G. Wang, *Appl. Surf. Sci.*, 2019, **493**, 551–560.
104 J. M. R. Narayanam and C. R. J. Stephenson, *Chem. Soc. Rev.*, 2011, **40**, 102–113.
105 P.-F. Wei, M.-Z. Qi, Z.-P. Wang, S.-Y. Ding, W. Yu, Q. Liu, L.-K. Wang, H.-Z. Wang, W.-K. An and W. Wang, *J. Am. Chem. Soc.*, 2018, **140**, 4623–4631.
106 X. Yan, H. Liu, Y. Li, W. Chen, T. Zhang, Z. Zhao, G. Xing and L. Chen, *Macromolecules*, 2019, **52**, 7977–7983.
107 C. Wang, Y. Meng, Y. Luo, J. L. Shi, H. Ding, X. Lang, W. Chen, A. Zheng and J. Sun, *Angew. Chem., Int. Ed.*, 2019, **59**, 3624–3629.
108 J. Alemán, S. Cabrera, R. Mas-Ballesté, A. Jiménez-Almarza, A. López-Magano and L. Marzo, *ChemCatChem*, 2019, **11**, 4916–4922.

109 Z. Li, Y. Zhi, P. Shao, H. Xia, G. Li, X. Feng, X. Chen, Z. Shi and X. Liu, *Appl. Catal., B*, 2019, **245**, 334–342.
110 Q. Zhang, I. Lee, J. B. Joo, F. Zaera and Y. Yin, *Acc. Chem. Res.*, 2013, **46**, 1816–1824.
111 W. Huang, Z. J. Wang, B. C. Ma, S. Ghasimi, D. Gehrig, F. Laquai, K. Landfester and K. A. I. Zhang, *J. Mater. Chem. A*, 2016, **4**, 7555–7559.
112 D. Sun, S. Jang, S.-J. Yim, L. Ye and D.-P. Kim, *Adv. Funct. Mater.*, 2018, **28**, 1707110.
113 Y. Zhi, Z. Li, X. Feng, H. Xia, Y. Zhang, Z. Shi, Y. Mu and X. Liu, *J. Mater. Chem. A*, 2017, **5**, 22933–22938.
114 W. Liu, Q. Su, P. Ju, B. Guo, H. Zhou, G. Li and Q. Wu, *ChemSusChem*, 2017, **10**, 664–669.
115 M. T. Schümperli, C. Hammond and I. Hermans, *ACS Catal.*, 2012, **2**, 1108–1117.
116 B. Chen, L. Wang and S. Gao, *ACS Catal.*, 2015, **5**, 5851–5876.
117 Z. Liu, Q. Su, P. Ju, X. Li, G. Li, Q. Wu and B. Yang, *Chem. Commun.*, 2020, **56**, 766–769.
118 M. Yoon, R. Srirambalaji and K. Kim, *Chem. Rev.*, 2012, **112**, 1196–1231.
119 X. Kang, X. Wu, X. Han, C. Yuan, Y. Liu and Y. Cui, *Chem. Sci.*, 2020, **11**, 1494–1502.
120 M. Tian, S. Liu, X. Bu, J. Yu and X. Yang, *Chem.–Eur. J.*, 2019, **26**, 369–373.
121 S. Liu, W. Pan, S. Wu, X. Bu, S. Xin, J. Yu, H. Xu and X. Yang, *Green Chem.*, 2019, **21**, 2905–2910.
122 P. Pachfule, A. Acharjya, J. Roeser, R. P. Sivasankaran, M.-Y. Ye, A. Brückner, J. Schmidt and A. Thomas, *Chem. Sci.*, 2019, **10**, 8316–8322.
123 S. Wang, Q. Sun, W. Chen, Y. Tang, B. Aguila, Y. Pan, A. Zheng, Z. Yang, L. Wojtas, S. Ma and F.-S. Xiao, *Matter*, 2019, **2**, 416–427.
124 M. Bhadra, S. Kandambeth, M. K. Sahoo, M. Addicoat, E. Balaraman and R. Banerjee, *J. Am. Chem. Soc.*, 2019, **141**, 6152–6156.
125 S. He, B. Yin, H. Niu and Y. Cai, *Appl. Catal., B*, 2018, **239**, 147–153.
126 H. Lv, X. Zhao, H. Niu, S. He, Z. Tang, F. Wu and J. P. Giesy, *J. Hazard. Mater.*, 2019, **369**, 494–502.
127 Y. Yao, Y. Hu, H. Hu, L. Chen, M. Yu, M. Gao and S. Wang, *J. Colloid Interface Sci.*, 2019, **554**, 376–387.
128 J. Pan, L. Guo, S. Zhang, N. Wang, S. Jin and B. Tan, *Chem.–Asian J.*, 2018, **13**, 1674–1677.
129 Y. Hou, C.-X. Cui, E. Zhang, J.-C. Wang, Y. Li, Y. Zhang, Y. Zhang, Q. Wang and J. Jiang, *Dalton Trans.*, 2019, **48**, 14989–14995.
130 Y. Zhang, Y. Hu, J. Zhao, E. Park, Y. Jin, Q. Liu and W. Zhang, *J. Mater. Chem. A*, 2019, **7**, 16364–16371.
131 Y. Peng, M. Zhao, B. Chen, Z. Zhang, Y. Huang, F. Dai, Z. Lai, X. Cui, C. Tan and H. Zhang, *Adv. Mater.*, 2018, **30**, 1705454.
132 S.-W. Lv, J.-M. Liu, C.-Y. Li, N. Zhao, Z.-H. Wang and S. Wang, *Chemosphere*, 2020, **243**, 125378.
133 S. He, Q. Rong, H. Niu and Y. Cai, *Appl. Catal., B*, 2019, **247**, 49–56.
134 L. P. Guo and S. B. Jin, *Chemphotochem*, 2019, **3**, 973–983.
135 F. Niu, L. Tao, Y. Deng, H. Gao, J. Liu and W. Song, *New J. Chem.*, 2014, **38**, 5695–5699.
136 S.-R. Zhu, Q. Qi, Y. Fang, W.-N. Zhao, M.-K. Wu and L. Han, *Cryst. Growth Des.*, 2018, **18**, 883–891.
137 W. Chen, Z. Yang, Z. Xie, Y. Li, X. Yu, F. Lu and L. Chen, *J. Mater. Chem. A*, 2019, **7**, 998–1004.
138 R. He, K. Xue, J. Wang, T. Yang, R. Sun, L. Wang, X. Yu, U. Omeoga, W. Wang, T. Yang, Y. Hu and S. Pi, *J. Mater. Sci.*, 2019, **54**, 14690–14706.